Solving time-harmonic Galbrun's equation with an arbitrary flow. Application to Helioseismology

Juliette Chabassier, Marc Duruflé

Solving time-harmonic Galbrun's equation with an arbitrary flow. Application to Helioseismology

Juliette Chabassier, Marc Duruflé

RESEARCH REPORT
N° 9192
May 2018
Project-Teams Magique-3D

ISSN 0249-6399 ISRN INRIA/RR--9192--FR+ENG

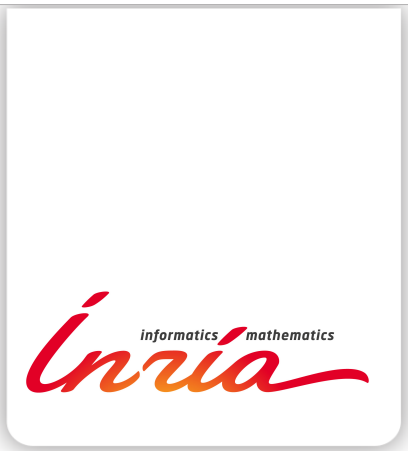

Solving time-harmonic Galbrun's equation with an arbitrary flow. Application to Helioseismology

Juliette Chabassier*, Marc Duruflé†

Project-Teams Magique-3D

Research Report n° 9192 — May 2018 — 52 pages

Abstract: In this report, we are concerned with the solution of Galbrun's equations in time-harmonic domain for an arbitrary flow with high order finite element methods. Several equivalent formulations of Galbrun's equations are proposed and discretized with Discontinuous Galerkin method. They are compared with a formulation adapted for continuous Galerkin discretization. Numerically, it has been observed that the tested discretization methods converge correctly for an uniform flow, but no longer for a non-uniform flow. Two kinds of stabilization are proposed in order to restore a nice convergence though original equations are modified. Finally, simplified Galbrun's equations are proposed to coincide with original Galbrun's equations when the flow is null. Numerical illustrations are presented in the context of helioseismology.

Key-words: Galbrun's equation, finite elements, axisymmetric geometry, helioseismology

* University of Pau, INRIA Bordeaux Sud-Ouest, EPI Magique 3-D
† Institute of Mathematics of Bordeaux, INRIA Bordeaux Sud-Ouest, EPI Magique 3-D

RESEARCH CENTRE
BORDEAUX – SUD-OUEST

200 avenue de la Vieille Tour
33405 Talence Cedex

Résolution de l'équation de Galbrun avec un flot quelconque. Application à l'héliosismologie.

Résumé : Dans ce document, nous nous intéressons à la résolution des équations de Galbrun en régime harmonique pour un écoulement quelconque par des méthodes d'éléments finis d'ordre élevé. Nous proposons plusieurs formulations équivalentes des équations de Galbrun discrétisées par une méthode de Galerkin discontinue, que nous comparons à une formulation adaptée aux éléments finis continus. Nous observons numériquement que les différentes méthodes de discrétisation testées convergent correctement pour un écoulement uniforme, mais ne convergent pas pour un écoulement non-uniforme. Nous proposons deux types de stabilisation qui bien que modifiant les équations initiales permettent de retrouver une convergence satisfaisante. Nous proposons aussi des équations de Galbrun simplifiées qui coïncident avec les équations de Galbrun originales lorsque l'écoulement est nul. Nous montrons des illustrations dans le contexte de l'héliosismologie.

Mots-clés : équation de Galbrun, éléments finis, héliosismologie, géométrie axisymétrique

Contents

1 General setting

1.1 Galbrun's equation

In this document, our main concern is to solve the Galbrun's equation:

$$\rho_0 \left(-i\omega + \sigma + M \cdot \nabla\right)^2 u - \nabla \left(\rho_0 \, c_0^2 \, \mathrm{div}\, u\right) + (\mathrm{div}\, u)\, \nabla p_0 - (\nabla u)^T \nabla p_0 \;=\; f \tag{1}$$

$u : \mathbb{R}^2 \to \mathbb{C}^2$ is the displacement (unknown), $\rho_0 \in \mathbb{R}$, $p_0 \in \mathbb{R}$, $c_0 \in \mathbb{R}$, $M \in \mathbb{R}^2$ are the background density, pressure, sound speed and flow velocity. These last quantities are given, they are in general obtained as solutions of non-linear steady hydrodynamic equations. σ is the damping coefficient, it might depend on the position (x, y). ω is the pulsation and $f \in \mathbb{R}^2$ the source. In our notations, the transpose of the gradient of u is equal to:

$$(\nabla u)^T \;=\; \begin{pmatrix} \partial_x u_x & \partial_x u_y \\ \partial_y u_x & \partial_y u_y \end{pmatrix}$$

Galbrun's equation is obtained by linearizing Euler's equation and considering the Lagragian displacement (see [13] for a derivation with gravity terms and rotation). For helioseismology applications, it is quite interesting to obtain directly this Lagrangian displacement (instead of the Eulerian displacement) since this is the displacement that is measured through Doppler's effect. In this report, gravity terms and rotation terms are not considered. Galbrun's equation is also known for aeroacoustics ([9], [12]). For that application, the background data (ρ_0, p_0, c_0, M) usually satisfy the steady Euler's equations (with null right hand-sides). However, in the case of helioseismology, the background data no longer satisfy these equations with null right-hand-sides, since the only solution would be the null solution. Therefore, there are some sources inside the sun, moreover additional terms (gravity terms, turbulence, coupling with magnetic field) can play the role of sources. Though Galbrun's equations are obtained by assuming a null right-hand-side, they will be used for a background that does not satisfy this assumption. That is why this report is supposed to deal with arbitrary flows that does not satisfy steady Euler's equations. In an inversion procedure, where the background data is recovered from physical measurements, it seems also simpler to not constrain the flow.

1.2 Linearized Euler's equation

The linearized Euler equations are obtained by considering Eulerian perturbations of non-linear Euler equations. They are given as

$$\begin{cases} (-i\omega + \sigma + M \cdot \nabla)\rho + \rho\, \mathrm{div}\,(M) + \mathrm{div}(u) = 0 \\ (-i\omega + \sigma + M \cdot \nabla)u + \nabla M(\rho M + u) - \dfrac{\nabla \rho_0 \cdot M}{\rho_0} u + \nabla p = g \\ (-i\omega + \sigma + M \cdot \nabla)p + (1-\gamma)\dfrac{u \cdot \nabla p_0}{\rho_0} + \mathrm{div}\left(c_0^2 u\right) + \gamma\, \mathrm{div}(M) p - p_0 \dfrac{\nabla \gamma \cdot u}{\rho_0} = 0 \end{cases} \tag{2}$$

where γ is given by

$$c_0^2 = \frac{\gamma p_0}{\rho_0}$$

These equations are introduced for example in [3], their derivation is explained in appendix B. In [3], the authors propose a simplified model that removes Kelvin-Helmholtz instabilities. This model is obtained by removing some terms under the assumption of a slowly varying flow and

uniform density ρ_0 and pressure p_0. This simplified model, that we call Bogey-Bailly-Juvé model, is given as

$$\begin{cases} (-i\omega + \sigma + M \cdot \nabla)p + \operatorname{div}(c_0^2\, u) = 0 \\ (-i\omega + \sigma + M \cdot \nabla)u + \nabla p = g \end{cases} \tag{3}$$

When the density ρ_0 and pressure p_0 are assumed constant, M has a null divergence (if the background satisfies steady Euler equations) and the following system is obtained (that we will call Simplified LEE):

$$\begin{cases} (-i\omega + \sigma + M \cdot \nabla)p + \operatorname{div}(c_0^2\, u) = 0 \\ (-i\omega + \sigma + M \cdot \nabla)u + \nabla p + (\nabla M)u = g \end{cases} \tag{4}$$

In the case of a uniform flow M, these equations give the same solution u as in equation (1), if we have the relation

$$f \;=\; (-i\omega + \sigma + M \cdot \nabla)g$$

Simplified LEE are popular since the equations are simpler, and only two unknowns p and u need to be solved. It can be noticed that Bogey-Bailly-Juvé model can be obtained from the simplified LEE by removing the term $(\nabla M)u$ in the second equation.

2 Discretization of Galbrun's equation

The computational domain Ω is meshed into quadrilaterals.

$$\Omega = \bigcup_{i=1}^{N} K_i$$

where K_i denotes a quadrilateral of the mesh. For axisymmetric configuration, only the section (in plane Orz) of the geometry is meshed. For example, a sphere will be reduced to a half-disc. The finite element space for an unknown u with m components is given as

$$U_h = \left\{ u \in (L^2(\Omega))^m \text{ such that } u \circ F_i \in (\mathbb{Q}_r)^m \right\}$$

where $\mathbb{Q}_r$ is the space of polynomials of degree lower or equal to r in each variable:

$$\mathbb{Q}_r = \operatorname{Span}\left\{ x^i y^j, \quad 1 \le i, j \le r \right\}$$

F_i is the transformation from the unit square $\hat{K} = [0,1]^2$ to the quadrilateral K_i (see figure 1).

2.1 Discontinuous Galerkin discretization

All the equations solved in this document will be linear and involve at most second-order derivatives in space. Therefore the general form of an equation is given as

$$A(x)u(x) - \operatorname{Div}\left(C(x)\nabla u(x) + D(x)u(x)\right) + E(x)\nabla u(x) = f(x)$$

where u comprises all the unknowns (p, ρ and u for LEE). $A(x), C(x), D(x)$ and $E(x)$ are tensors that depend continuously on the variable x. In the context of helioseismology, we assume that the physical background does not have discontinuity. For example $A(x)$ will be a matrix whereas

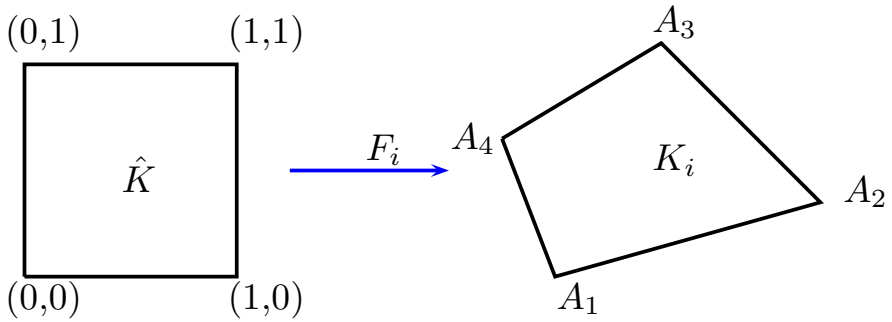

Figure 1: Transformation F_i for a quadrilateral.

$C(x)$ will be a tensor (with four indices i, j, k, l), $D(x)$ and $E(x)$ tensors with three indices. We use the following notations

$$(C(x)\nabla u(x))_{i,j} = \sum_{k,l} C_{i,j,k,l}(x)\frac{\partial u_k(x)}{\partial x_l}$$

$$(D(x)u(x))_{i,j} = \sum_{k} D_{i,j,k}(x)u_k(x)$$

$$(E(x)\nabla u(x))_{k} = \sum_{i,j} E_{i,j,k}(x)\frac{\partial u_i(x)}{\partial x_j}$$

The transpose of $E(x)$ is defined as

$$(E^T(x)v)_{i,j} = \sum_{k} E_{i,j,k}(x)v_k$$

The gradient of a vector and the divergence of a matrix are defined as

$$\nabla u(x) = \frac{\partial u_i}{\partial x_j}, \quad \text{Div}\, A(x) = \sum_j \frac{\partial A_{i,j}}{\partial x_j}$$

To obtain the variational formulation, the equation is multiplied by a test-function v, integrated over an element K of the mesh and integration by parts is performed to obtain :

$$\int_K A(x)u(x)v(x)\,dx+$$
$$\int_K (C(x)\nabla u(x) + D(x)u(x)) : \nabla v(x)\,dx - \int_{\partial K} \{C(x)\nabla u(x) + D(x)u(x)\}\, n(x)\cdot v(x)\,dx$$
$$-\int_K u(x)\cdot \text{Div}\left(E^T(x)v(x)\right)\,dx + \int_{\partial K} \{u(x)\}\cdot E^T(x)v(x)n(x)\,dx = \int_K f(x)\cdot v(x)\,dx$$

where $n(x)$ is the outgoing normale to element K. The component-wise inner product of two matrices is denoted : and given as

$$A : B = \sum_{i,j} A_{i,j}B_{i,j}$$

For the numerical fluxes, we have chosen centered fluxes by noting

$$\{u\} = \frac{1}{2}(u_1 + u_2)$$

where u_1 and u_2 are the values of u across the interface ∂K. We also note

$$[u] = u_2 - u_1$$

with the convention that the normale $n(x)$ is outgoing from element K_1 to element K_2. The integrals for each element are summed in order to regroup boundary integrals together, and integration by parts is performed for the term $\mathrm{Div}\left(E^T(x)v(x)\right)$, in order to obtain :

$$\begin{aligned}
&\sum_{K \text{ element of } \Omega} \int_K A(x)u(x)\cdot v(x) + (C(x)\nabla u(x) + D(x)u(x)) : \nabla v(x) + E(x)\nabla u(x)\cdot v(x)\, dx \\
+ &\sum_{e \text{ edge of } \Omega} \int_e \{C(x)\nabla u(x) + D(x)u(x)\}\, n(x)\cdot[v(x)] + [u(x)]\cdot\left\{E^T(x)v(x)\right\} n(x)\, dx \\
&= \sum_{K \text{ element of } \Omega} \int_K f(x)\cdot v(x)\, dx
\end{aligned}$$

In order to obtain a stable symmetric formulation (as done for the wave equation [10]), we add a term with $[u]$ which is null for the exact solution (since operators $A(x), C(x), D(x)$ and $E(x)$ are continuous), and also a penalty term, to obtain the final variational formulation

$$\begin{aligned}
&\sum_{K \text{ element of } \Omega} \int_K A(x)u(x)\cdot v(x) + (C(x)\nabla u(x) + D(x)u(x)) : \nabla v(x) + E(x)\nabla u(x)\cdot v(x)\, dx \\
+ &\sum_{e \text{ edge of } \Omega} \int_e \{C(x)\nabla u(x)\}\, n(x)\cdot[v(x)] + \{C(x)\nabla v(x)\}\, n(x)\cdot[u(x)] \\
&\qquad + \{D(x)u(x)\}\, n(x)\cdot[v(x)] + [u(x)]\cdot\left\{E^T(x)v(x)\right\} n(x)\, dx + \frac{1}{2}P(x)[u(x)]\cdot[v(x)]\, dx \\
&= \sum_{K \text{ element of } \Omega} \int_K f(x)\cdot v(x)\, dx
\end{aligned} \tag{5}$$

where $P(x)$ is a penalty matrix that depends on the background data. If Helmholtz equation is considered (u is scalar), then we recover the interior penalty formulation proposed by Grote and coworkers ([10]), by chosing P as:

$$P(x) = \alpha\frac{r(r+1)}{h^2} \tag{6}$$

where h is the length of the considered edge. When $C(x) = 0$ (i.e. we have a first-order formulation), we recover the classical DG method (see [11] for Maxwell's equations) with centered fluxes if $P = 0$ and with upwind fluxes if P is chosen as:

$$P(x) = |B_n|$$

where $|B_n|$ denotes here the absolute value of the square matrix B_n defined as

$$(B_n)_{i,j} = \sum_j D_{i,j,k}(x)n_j(x) + E_{i,j,k}(x)n_j(x)$$

We assume that the constant operator $A(x)$ can be decomposed as

$$A(x) = -i\omega M(x) + A_0(x)$$

The absolute value is here defined through the eigenvalue decomposition of the matrix $M(x)^{-1}B_n$. If this matrix is diagonalizable, we have

$$M(x)^{-1}B_n(x) = V\Lambda V^{-1}$$

where V contains the eigenvectors of $M(x)^{-1}B_n(x)$ and Λ the eigenvalues. The absolute matrix of B_n is defined by

$$|B_n| = M(x)V|\Lambda|V^{-1}$$

where $|\Lambda|$ is the diagonal matrix with absolute values of eigenvalues. In the appendix A, the absolute value of the matrices B_n is given for the different equations considered in this document. It should be noted that a zero-order absorbing boundary condition is also constructed from this computation of the absolute value of B_n (see [2]). The unknown u is discretized with the finite element space U_h, for the basis functions we are choosing Gauss-Lobatto points to obtain Lagrange interpolation polynomials (see [6]). For the integrals, we have chosen to compute them with Gauss-Legendre points (instead of Gauss-Lobatto points) in order to have an accurate integration.

A first solution to solve Galbrun's equations (1) is to use the variational formulation (5) directly. We choose the following penalty matrix

$$P(x) = \alpha\frac{r(r+1)}{h^2}\rho_0(x)c_0^2(x)n(x)n(x)^T \tag{7}$$

The presence of n is here due to the particular form of Galbrun's equation when the flow M is null. If $M = 0$, the natural space for u is $H(div, \Omega)$, and $u \cdot n$ is the quantity that is continuous across edges. The obtained method will be called Symmetric Interior Penalty Galerkin (SIPG), since the finite element matrix hence obtained is symmetric for a null flow. By choosing α large enough, the stiffness matrix is positive (for a flow M null), and the method is spurious-free by using triangles. The use of quadrilaterals give some spurious eigenmodes, because the local polynomial space $\mathbb{Q}_r^2$ is the same as elements of the second kind (among Nédélec's families). A solution would be to use the local polynomial space of the first kind ($\mathbb{Q}_{r,r-1} \times \mathbb{Q}_{r-1,r}$ for H(div) quadrilaterals). With this choice, the method would also be spurious-free for quadrilaterals.

2.2 Alternative formulations for Galbrun's equation

2.2.1 Formulation PV

In this formulation, two unknowns p and v are added to obtain the following system:

$$\begin{cases} \rho_0\left(-i\omega + \sigma + M\cdot\nabla\right)u - \rho_0 v = 0 \\ \rho_0\left(-i\omega + \sigma + M\cdot\nabla\right)v - \nabla(\rho_0\, c_0^2\, p) + p\nabla p_0 - (\nabla u)^T\nabla p_0 = f \\ p - \operatorname{div} u = 0 \end{cases} \tag{8}$$

We obtain a first-order formulation (with only first-order derivatives in time and space), that is discretized with DG formulation (5). However, this formulation does not have the same form of an hyperbolic system

$$-i\omega u + A_x\partial_x u + A_y\partial_y u = 0$$

such that we cannot use our method to compute the absolute value of matrix B_n. For this formulation, if an upwind flux is selected, we have chosen the following penalty matrix

$$P(x) \;=\; \alpha \begin{pmatrix} 0 & 0 & 0 \\ -i\,\omega\rho_0 c_0\, nn^T & 0 & 0 \\ 0 & 0 & \dfrac{ic_0}{\omega} \end{pmatrix}$$

The value $\alpha = 1$ corresponds to an upwind flux for a null flow (since it corresponds to a zero-order absorbing boundary condition).

2.2.2 Formulation PQ

In this formulation, two unknowns p and q are added to obtain the following system:

$$\begin{cases} \rho_0\,(-i\omega + \sigma + M\cdot\nabla)\,u - \nabla p - \rho_0\, q = 0 \\ \rho_0\,(-i\omega + \sigma + M\cdot\nabla)\,q - (\nabla\sigma)\,p - (\nabla M)^T\nabla p - \dfrac{M\cdot\nabla\rho_0}{\rho_0}\nabla p + (\operatorname{div} u)\nabla p_0 - (\nabla u)^T\nabla p_0 = f \\ \rho_0\,(-i\omega + \sigma + M\cdot\nabla)\,p - \rho_0^2\, c_0^2 \operatorname{div} u = 0 \end{cases} \tag{9}$$

The equivalence with the equation (1) is obtained by dividing the first equation by ρ_0 then by applying the operator $\rho_0\,(-i\omega + \sigma + M\cdot\nabla)$. The permutation between ∇ and $(-i\omega + \sigma + M\cdot\nabla)$ give the terms $(\nabla\sigma)\,p + (\nabla M)^T\nabla p + \dfrac{M\cdot\nabla\rho_0}{\rho_0}\nabla p$. This formulation is also a first-order formulation discretized with discontinuous Galerkin formulation (5). Contrary to the formulation (8), this form is similar to the formulation of an hyperbolic system. However, the matrix B_n is not diagonalizable. In the appendix (A), we propose to compute the absolute value by considering a sequence of diagonalizable matrices that tends to B_n.

2.2.3 Formulation H1

This formulation has been proposed in [4], [5], in which it has been proven equivalent to equation (1). It is relevant for σ constant, and if $p_0 = g(\rho_0)$ then the following compatibility condition must be satisfied

$$c_0^2 = g'(\rho_0).$$

For this formulation, the flow M will be assumed to satisfy the following constraint:

$$\operatorname{div}(\rho_0 M) = 0$$

This hypothesis allows us to make integration by parts on terms involving M without obtaining a residual term with the divergence of $\rho_0 M$. An additional unknown ψ (which is the curl of u) has been introduced.

$$\begin{cases} \rho_0\,(-i\omega + \sigma + M\cdot\nabla)^2\,u - \nabla\left(\rho_0 c_0^2 \operatorname{div} u\right) + \operatorname{curl}\left(\rho_0 c_0^2\,(\operatorname{curl}(u) - \psi)\right) + (\operatorname{div} u)\nabla p_0 - (\nabla u)^T\nabla p_0 = f \\ \rho_0\,(-i\omega + \sigma + M\cdot\nabla)^2\,\psi = -2\rho_0\,(-i\omega + \sigma + M\cdot\nabla)\,(\mathcal{B}u) - \rho_0\,\mathcal{C}(u) + \operatorname{curl}(f) + \dfrac{1}{\rho_0 c_0^2} f\wedge\nabla p_0 \end{cases} \tag{10}$$

where

$$\mathcal{B}(u) = \sum_{j=1}^{2} \nabla M_j \wedge \frac{\partial u}{\partial x_j}$$

$$\mathcal{C}(u) = \sum_{j,k=1}^{2} \left(\frac{\partial M_k}{\partial x_j} \nabla M_j \wedge \frac{\partial u}{\partial x_k} - M_j \nabla \frac{\partial M_k}{\partial x_j} \wedge \frac{\partial u}{\partial x_k} \right) + \frac{1}{\rho_0} \sum_{j=1}^{2} \left(\frac{1}{\rho_0 c_0^2} \frac{\partial p_0}{\partial x_j} \nabla p_0 - \nabla \left(\frac{\partial p_0}{\partial x_j} \right) \right) \wedge \nabla u_j$$

The purpose of the added curl $\left(\rho_0 c_0^2 \left(\mathrm{curl}(u) - \psi\right)\right)$ term is to restore the coercivity of the bilinear form. This is achieved for low-mach number. The variational formulation is given by (with periodic boundary condition) :

$$\begin{aligned}
&\int_\Omega \rho_0 \left(-i\omega + \sigma\right)^2 u \cdot v + 2\rho_0(-i\omega+\sigma) M \cdot \nabla u \cdot v - \rho_0 (M \cdot \nabla u) \cdot (M \cdot \nabla v)\, dx \\
&+ \int_\Omega \rho_0 c_0^2 \left(\mathrm{div}\, u \,\mathrm{div}\, v + (\mathrm{curl}(u) - \psi)\,\mathrm{curl}(v)\right) + (\mathrm{div}\, u) \nabla p_0 \cdot v - (\nabla u)^T \nabla p_0 \cdot v \, dx \\
&+ \int_\Omega \rho_0 \Big[(-i\omega+\sigma)^2 \psi\, \tilde{\psi} + 2(-i\omega+\sigma) M \cdot \nabla \psi\, \tilde{\psi} - M \cdot \nabla \psi\, M \cdot \nabla \tilde{\psi} \\
&\qquad + 2(-i\omega+\sigma) \left(\frac{\partial m_x}{\partial x} \frac{\partial u_y}{\partial x} + \frac{\partial m_y}{\partial x} \frac{\partial u_y}{\partial y} - \frac{\partial m_x}{\partial y} \frac{\partial u_x}{\partial x} - \frac{\partial m_y}{\partial y} \frac{\partial u_x}{\partial y} \right) \tilde{\psi} \\
&\qquad + \left(\left(\frac{\partial m_x}{\partial x} \right)^2 + \frac{\partial m_y}{\partial x} \frac{\partial m_x}{\partial y} \right) \frac{\partial u_y}{\partial x}\, \tilde{\psi} + \left(\frac{\partial m_x}{\partial x} \frac{\partial m_y}{\partial x} + \frac{\partial m_y}{\partial x} \frac{\partial m_y}{\partial y} \right) \frac{\partial u_y}{\partial y}\, \tilde{\psi} \\
&\qquad - \left(\frac{\partial m_x}{\partial y} \frac{\partial m_x}{\partial x} + \frac{\partial m_y}{\partial y} \frac{\partial m_x}{\partial y} \right) \frac{\partial u_x}{\partial x}\, \tilde{\psi} - \left(\frac{\partial m_x}{\partial y} \frac{\partial m_y}{\partial x} + \left(\frac{\partial m_y}{\partial y} \right)^2 \right) \frac{\partial u_x}{\partial y}\, \tilde{\psi} \\
&\qquad - \left(m_x \frac{\partial^2 m_x}{\partial x^2} + m_y \frac{\partial^2 m_x}{\partial x \partial y} \right) \frac{\partial u_y}{\partial x}\, \tilde{\psi} - \left(m_x \frac{\partial^2 m_y}{\partial x^2} + m_y \frac{\partial^2 m_y}{\partial x \partial y} \right) \frac{\partial u_y}{\partial y}\, \tilde{\psi} \\
&\qquad + \left(m_x \frac{\partial^2 m_x}{\partial x \partial y} + m_y \frac{\partial^2 m_x}{\partial y^2} \right) \frac{\partial u_x}{\partial x}\, \tilde{\psi} + \left(m_x \frac{\partial^2 m_y}{\partial x \partial y} + m_y \frac{\partial^2 m_y}{\partial y^2} \right) \frac{\partial u_x}{\partial y}\, \tilde{\psi} \\
&\qquad - 2m_x \frac{\partial m_x}{\partial x} \frac{\partial \tilde{\psi}}{\partial x} \frac{\partial u_y}{\partial x} - 2m_y \frac{\partial m_x}{\partial x} \frac{\partial \tilde{\psi}}{\partial y} \frac{\partial u_y}{\partial x} - 2m_x \frac{\partial m_y}{\partial x} \frac{\partial \tilde{\psi}}{\partial x} \frac{\partial u_y}{\partial y} - 2m_y \frac{\partial m_y}{\partial x} \frac{\partial \tilde{\psi}}{\partial y} \frac{\partial u_y}{\partial y} \\
&\qquad + 2m_x \frac{\partial m_x}{\partial y} \frac{\partial \tilde{\psi}}{\partial x} \frac{\partial u_x}{\partial x} + 2m_y \frac{\partial m_x}{\partial y} \frac{\partial \tilde{\psi}}{\partial y} \frac{\partial u_x}{\partial x} + 2m_x \frac{\partial m_y}{\partial y} \frac{\partial \tilde{\psi}}{\partial x} \frac{\partial u_x}{\partial y} + 2m_y \frac{\partial m_y}{\partial y} \frac{\partial \tilde{\psi}}{\partial y} \frac{\partial u_x}{\partial y} \Big]\, dx \\
&+ \int_\Omega \frac{1}{\rho_0 c_0^2} \Big[- \frac{\partial p_0}{\partial x} \frac{\partial p_0}{\partial y} \frac{\partial u_x}{\partial x} + \left(\frac{\partial p_0}{\partial x} \right)^2 \frac{\partial u_x}{\partial y} - \left(\frac{\partial p_0}{\partial y} \right)^2 \frac{\partial u_y}{\partial x} + \frac{\partial p_0}{\partial y} \frac{\partial p_0}{\partial x} \frac{\partial u_y}{\partial y} \Big] \tilde{\psi}\, dx \\
&+ \int_\Omega \Big[\frac{\partial^2 p_0}{\partial x \partial y} \frac{\partial u_x}{\partial x} - \frac{\partial^2 p_0}{\partial x^2} \frac{\partial u_x}{\partial y} + \frac{\partial^2 p_0}{\partial y^2} \frac{\partial u_y}{\partial x} - \frac{\partial^2 p_0}{\partial x \partial y} \frac{\partial u_y}{\partial y} \Big] \tilde{\psi}\, dx \;=\; \int_\Omega \left[\mathrm{curl}(f) + \frac{1}{\rho_0 c_0^2} f \wedge \nabla p_0 \right] \tilde{\psi}\, dx
\end{aligned} \tag{11}$$

where $\tilde{\psi}$ is the test-function associated with ψ. If continuous finite elements are used, i.e. u belongs to the following finite element space

$$\widetilde{U}_h = \left\{ u \in (H^1(\Omega))^m \text{ such that } u \circ F_i \in (\mathbb{Q}_r)^m \right\}$$

and the variational formulation (11), this choice will be called formulation H1. If discontinuous finite elements are used, we have chosen to introduce an additional unknown φ given as

$$(-i\omega + \sigma + M \cdot \nabla)\psi = \varphi$$

such that the considered system is equal to

$$\begin{cases} \rho_0 \left(-i\omega + \sigma + M \cdot \nabla\right)^2 u - \nabla \left(\rho_0 c_0^2 \operatorname{div} u\right) + \operatorname{curl} \left(\rho_0 c_0^2 \ (\operatorname{curl}(u) - \psi)\right) + (\operatorname{div} u)\nabla p_0 - (\nabla u)^T \nabla p_0 = f \\ \rho_0 \left(-i\omega + \sigma + M \cdot \nabla\right) \varphi = -2\rho_0 \left(-i\omega + \sigma + M \cdot \nabla\right) (\mathcal{B}u) - \rho_0 \, \mathcal{C}(u) + \operatorname{curl}(f) + \dfrac{1}{\rho_0 c_0^2} f \wedge \nabla p_0 \\ \rho_0(-i\omega + \sigma + M \cdot \nabla)\psi - \rho_0 \, \varphi = 0 \end{cases} \tag{12}$$

The overall system (12) is solved with the variational formulation (5). The penalty matrix P is a mix between SIPG penalization terms for u (to ensure a positive stiffness matrix for a null flow) and upwind fluxes for the two advection equations in φ and ψ. Namely, we have taken

$$P(x) = \begin{pmatrix} \dfrac{\alpha\rho_0 c_0^2 r(r+1)}{h^2} & 0 & 0 & 0 \\ 0 & \dfrac{\alpha\rho_0 c_0^2 r(r+1)}{h^2} & 0 & 0 \\ 0 & 0 & \rho_0 |M \cdot n| & 0 \\ 0 & 0 & 0 & \rho_0 |M \cdot n| \end{pmatrix}$$

where α is large enough to ensure a positive stiffness matrix (usually we take 10). This choice of formulation is called formulation H1(DG).

3 Numerical convergence

The aim of the section is to compare the different methods that have been described in the previous section to solve Galbrun's equation : SIPG (1), formulation PV (8), formulation PQ (9), formulation H1 (10) and formulation H1(DG) (12). All these formulations are equivalent in continuous, they should provide the same solution after discretization. If it is not specified, upwind fluxes are used, and $\mathbb{Q}_{10}$ finite elements are used. The linear systems issued from the variational formulation (5) or (11) will be solved with the direct solver MUMPS [1].

3.1 Uniform flow

The computational domain is the square $[-4,4]^2$ with periodic boundary conditions. We choose a gaussian source centered at the origin:

$$f(x,y) = \sqrt{\frac{\alpha}{\pi}}\exp(-\alpha(x^2+y^2))$$

The constant α is chosen such that f is equal to 10^{-6} at the radius r_0:

$$\alpha = \frac{\log(10^6)}{r_0^2}$$

The radius r_0 is chosen equal to 1 here. We chose an uniform background:

$$M=(m_x,0), \quad \rho_0 = 2.5, \quad c_0 = 0.8, \quad p_0 = 1, \quad \omega = 0.78\times 2\,\pi, \quad \sigma = 0.1$$

The reference solutions are computed with formulation PQ, $r=12$, a regular mesh with $N=51$ points on each direction. The solution is displayed in figures 2, 3 and 4 for different values

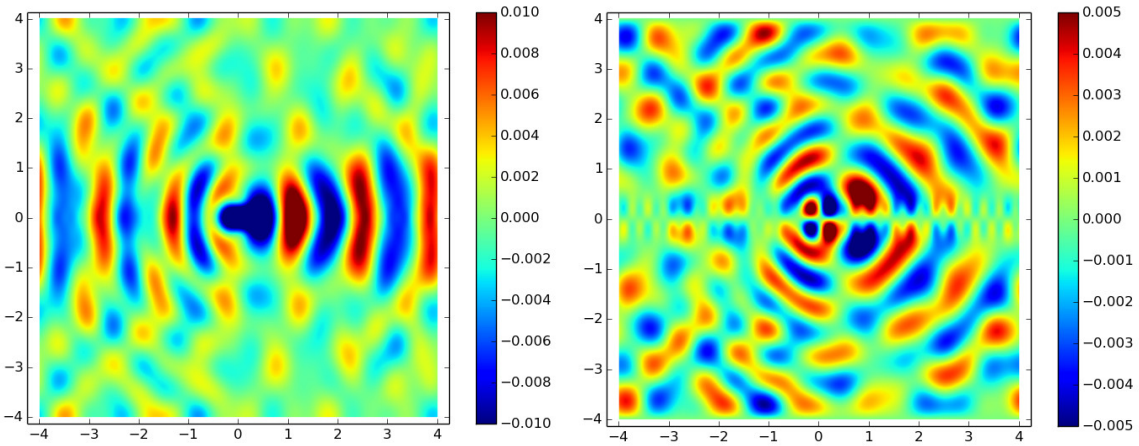

Figure 2: Real part of u_x (left) and u_y (right) for an uniform flow $m_x = 0.25$

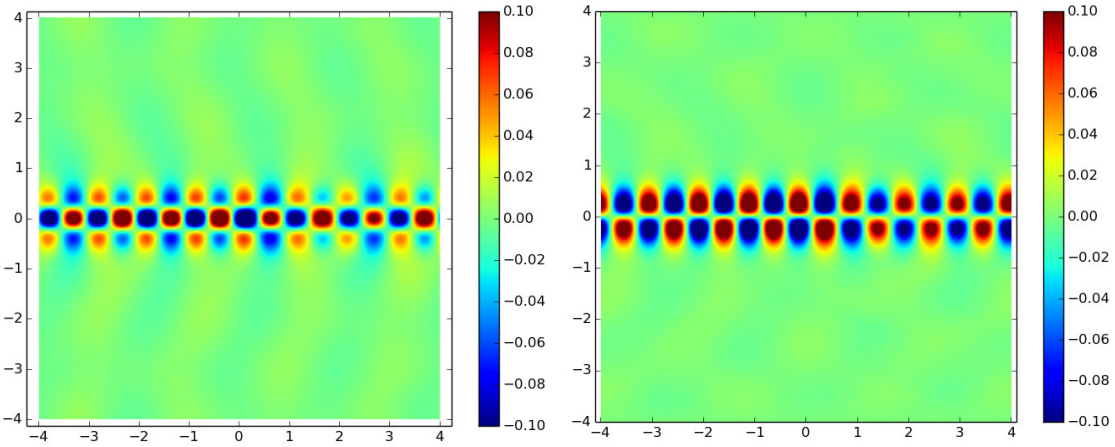

Figure 3: Real part of u_x (left) and u_y (right) for an uniform flow $m_x = 0.75$

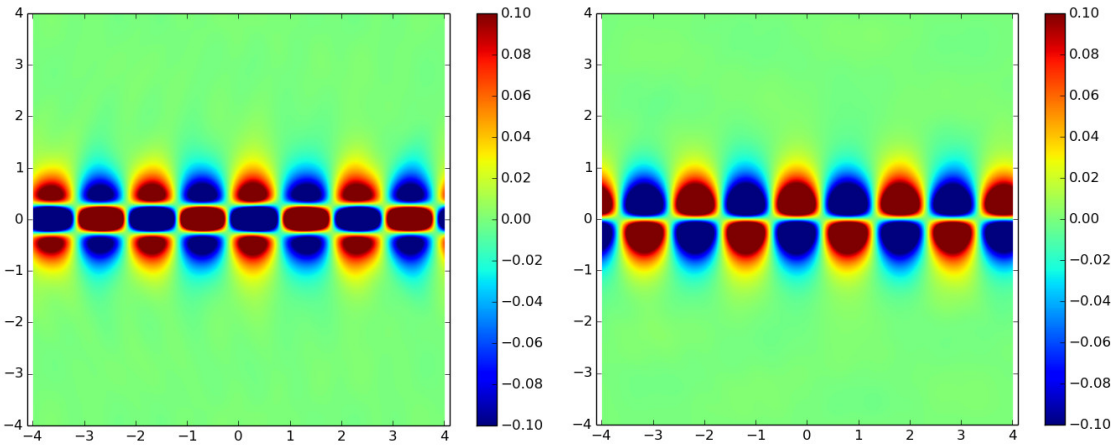

Figure 4: Real part of u_x (left) and u_y (right) for an uniform flow $m_x = 1.5$

of m_x. The vortex wave dominates for $m_x = 0.75$ and $m_x = 1.5$. The vortex wave has a wavelength equal to m_x, therefore the mesh must be fine enough (at least locally, close to the axis $y = 0$ in our example) to capture this wave when m_x is small. In figure 5, the relative L^2 error (computed on the main unknown u) is displayed for the formulation PQ versus the mesh size h divided by the order of approximation r. The numerical method converges in $O(h^{r+1})$ as expected. In figure 6, we have displayed the relative L^2 error obtained with $r = 5$ and $m_x = 0.25$ for different formulations of Galbrun's equations. The formulations where upwind fluxes have been implemented (PQ and H1(DG)) provide results more accurate than other formulations (SIPG, PV or H1). In figure 7, the L^2 error is displayed versus h/r for different values of m_x (formulation PQ is chosen). We observe a nice convergence in $O(h^{r+1})$ for these values of m_x. In

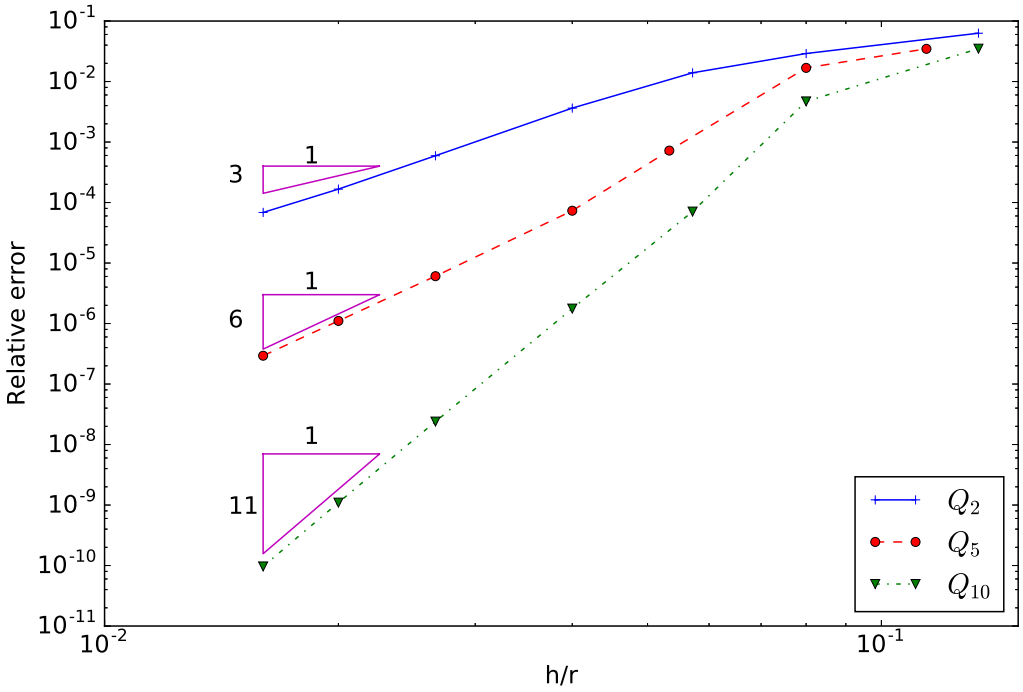

Figure 5: Relative L^2 error for formulation PQ versus h/r for different orders of approximation ($r = 2, 5, 10$). Case of an uniform flow with $m_x = 0.25$.

this sub-section, the numerical results show that the different formulations converge accurately towards the same solution.

3.2 Non-uniform flow

In this section, the source g is a gaussian centered at the origin with a radius of distribution equal to 1, and polarized in the x-direction. The source f is given as :

$$f \;=\; (-i\omega + \sigma + M \cdot \nabla)g$$

such that the solution obtained for Galbrun's equation can be compared qualitatively with solutions obtained with LEE equation. The computational domain is the square $[-4, 4]^2$ with periodic boundary conditions. Physical coefficients are chosen periodic :

$$\rho_0 = 1.5 + 0.2 \cos\left(\frac{\pi x}{4}\right) \sin\left(\frac{\pi y}{2}\right)$$

$$p_0 = 1.44\rho_0 + 0.08\rho_0^2$$

$$c_0^2 = 1.44 + 0.16\rho_0$$

$$\omega = 0.78 \times 2\,\pi, \quad \sigma = 0.1$$

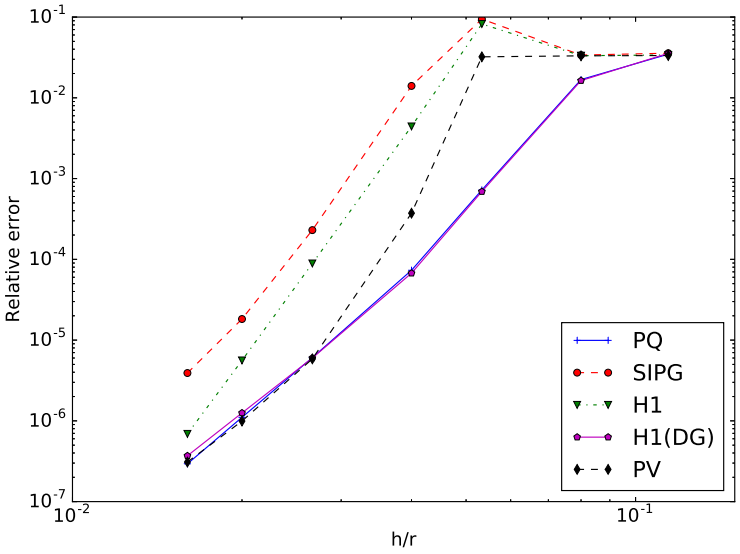

Figure 6: Relative L^2 error for different formulations versus h/r for $r = 5$. Case of an uniform flow with $m_x = 0.25$.

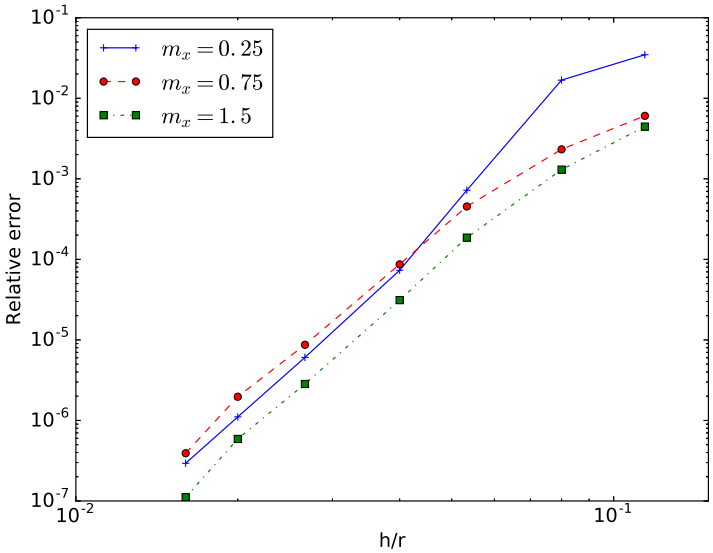

Figure 7: Relative L^2 error for different values of m_x versus h/r for $r = 5$. Case of an uniform flow, formulation PQ.

The flow M is given as:

$$m_x = \text{coeff}\left(\frac{0.3 + 0.1\cos\left(\frac{\pi y}{4}\right)}{\rho_0}\right)$$

$$m_y = \text{coeff}\left(\frac{0.2 + 0.08\sin\left(\frac{\pi x}{4}\right)}{\rho_0}\right)$$

The coefficient coeff will be specified in the different numerical simulations. The reference solutions are computed with the formulation $H1$, with $r = 12$ and a regular mesh with $N = 51$ points in each direction. However, with this choice, we have observed spurious oscillations in the solution (see figure 8) for coeff $= 0.2$. As a result, for this value of coefficient, we have computed

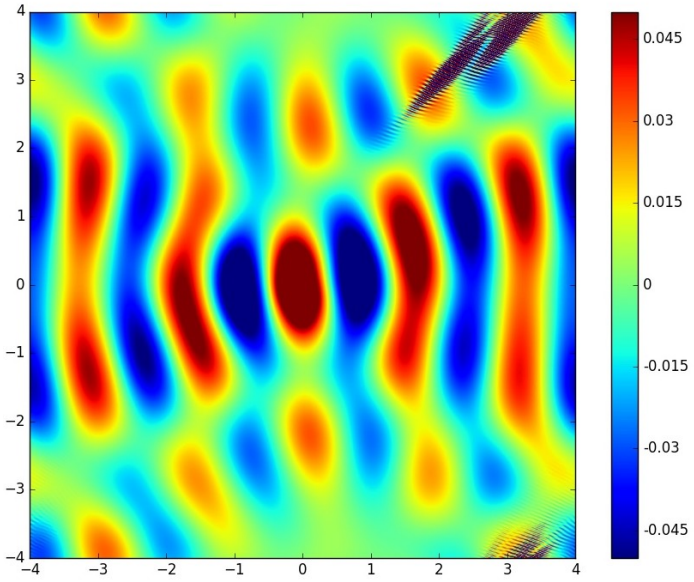

Figure 8: Numerical solution obtained with H^1 formulation (quadrilateral elements), with $N = 51$ points and $r = 12$ for a non-uniform flow (coeff $= 0.2$).

the reference solution with $r = 8$ and $N = 61$ points. We have observed this kind of spurious oscillations for other formulations (not only the formulation $H1$), when the number of points is increased or when the order of approximation r is increased. We think that the reason is that the finite element matrix becomes very ill-conditioned for finer meshes (or higher order approximation), the direct solver is no longer able to compute the solution accurealy. The solutions obtained for the references solutions are displayed in figures 9, 10, 11 and 12 for different values of coeff. In figure 13, the relative L^2 error is represented versus h/r for different values of coeff for the fomulation H1. We have also computed the consistency error defined as

$$\text{Consistency error} = \frac{||S_1 - S_2||}{||S_1||} \tag{13}$$

where the L_2 norm is used on the square $[-4, 4]$ stripped from the disk of center 0 and radius 1.5 such that the source f is not involved. The terms S_1 and S_2 are given as

$$S_1 = \rho_0 \left(-i\omega + \sigma + M \cdot \nabla\right)^2 u$$

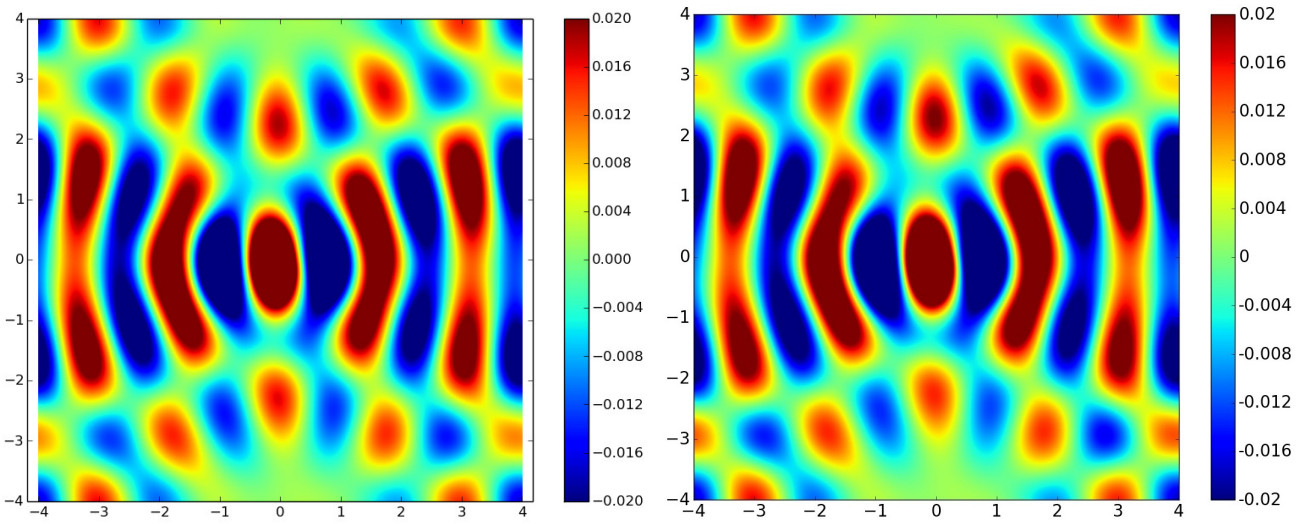

Figure 9: Solution obtained with Galbrun's equation (left) and LEE (right) (coeff = 0.1, real part of u_x).

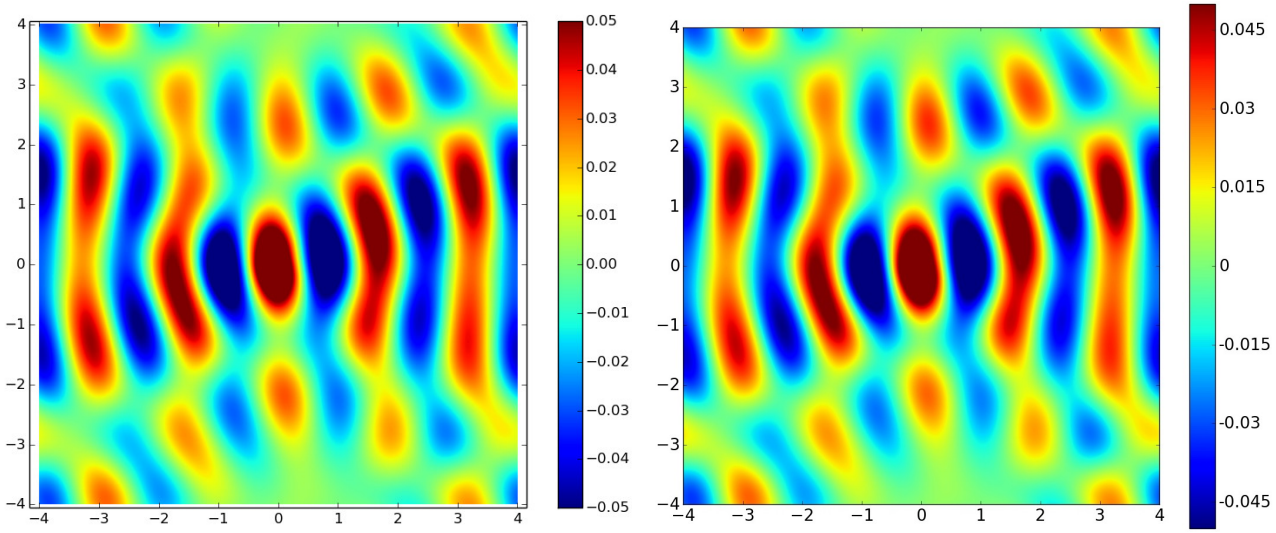

Figure 10: Solution obtained with Galbrun's equation (left) and LEE (right) (coeff = 0.2, real part of u_x).

$$S_2 = \nabla\left(\rho_0\, c_0^2\, \mathrm{div}\, u\right) - (\mathrm{div}\, u)\, \nabla p_0 + (\nabla u)^T \nabla p_0$$

We observe that the numerical method does not converge for any value of coeff and that the reached level of accuracy depends on coeff. For small values of coeff, the accuracy obtained on the solution is satisfying, while for larger values of coeff, the accuracy is very poor. We also observe a lack of robustness, that is to say that the numerical method may provide a large error for a very fine mesh. We have observed the same issue : lack of convergence and robustness for other formulations of Galbrun's equations. In figures 14, 15, 16 and 17, the relative L^2 error and

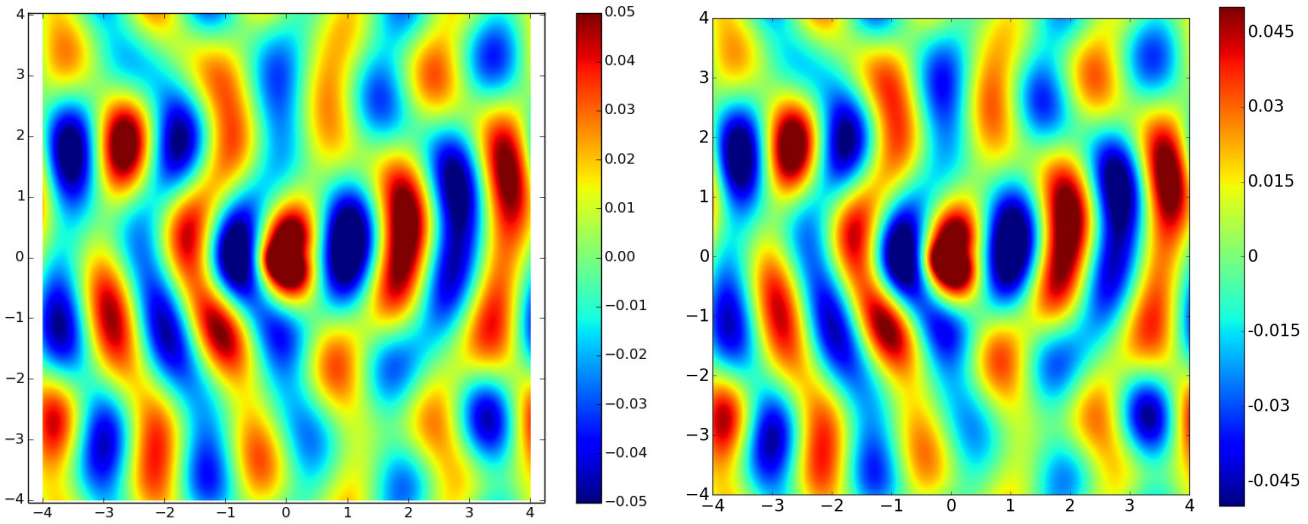

Figure 11: Solution obtained with Galbrun's equation (left) and LEE (right) (coeff = 0.5, real part of u_x).

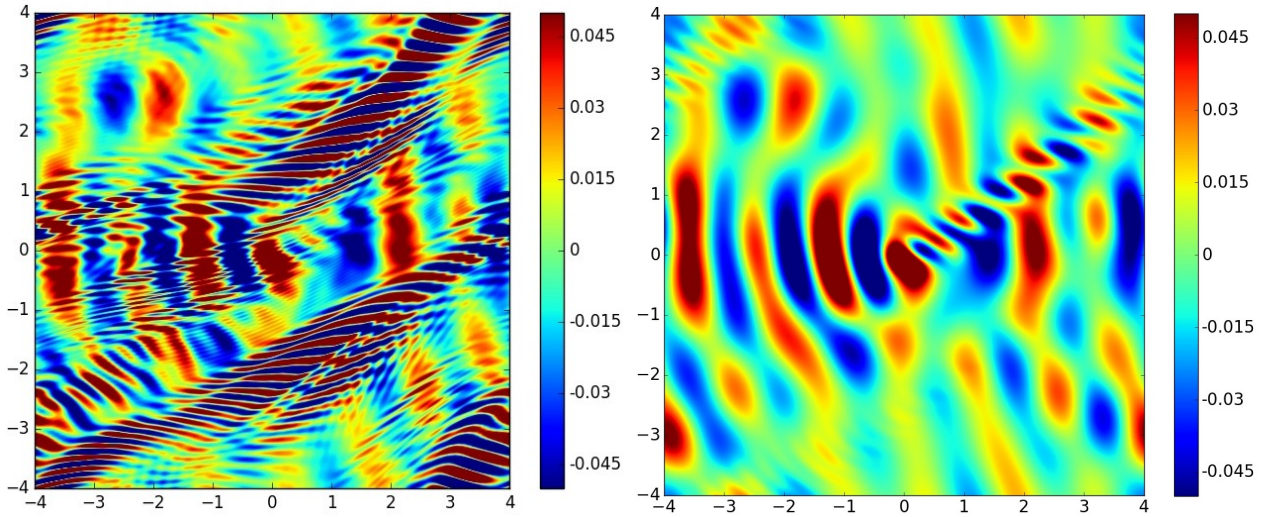

Figure 12: Solution obtained with Galbrun's equation (left) and LEE (right) (coeff = 1.5, real part of u_x).

consistency error are displayed versus h/r for the different formulations detailed in the previous section.

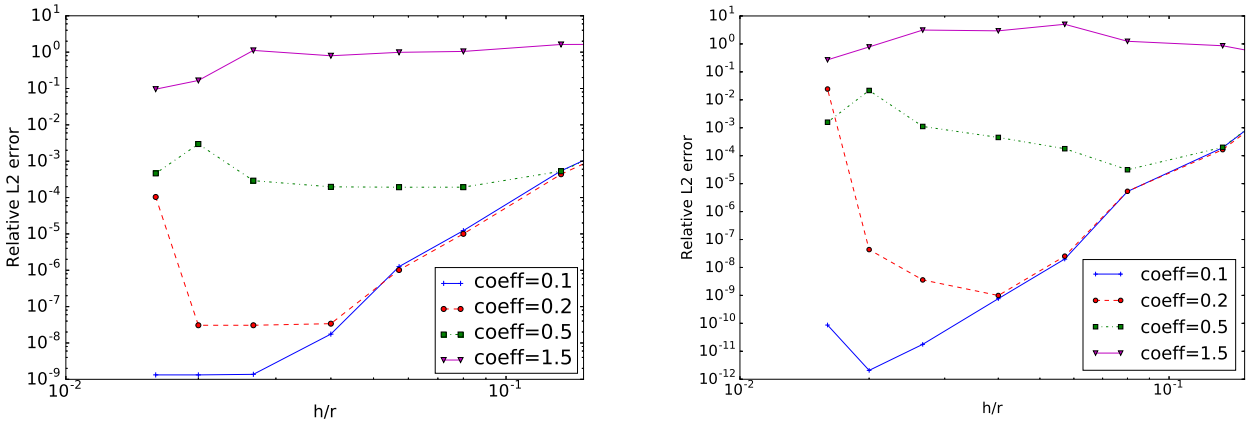

Figure 13: Relative L^2 error (left) and consistency error (right) versus h/r for formulation H1 and different values of coeff. Case of a non-uniform flow.

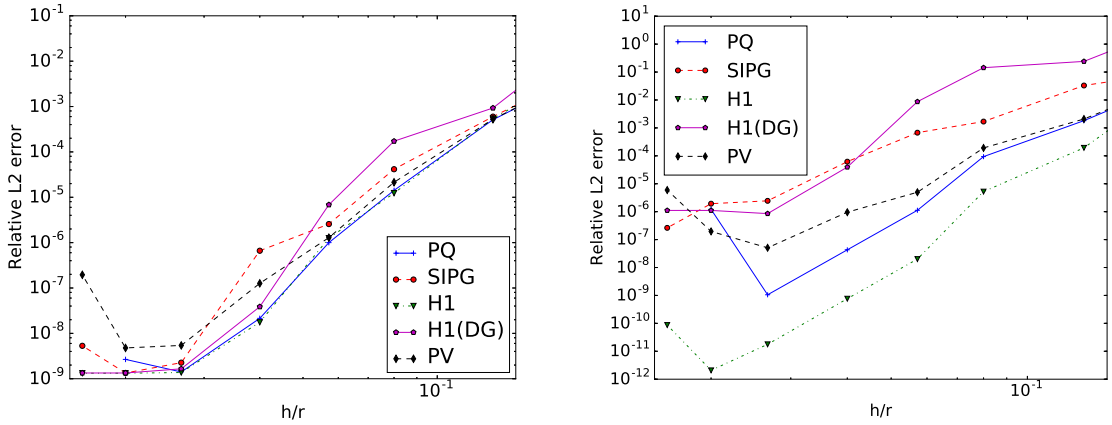

Figure 14: Relative L^2 error (left) and consistency error (right) versus h/r for coeff=0.1 and different formulations. Case of a non-uniform flow.

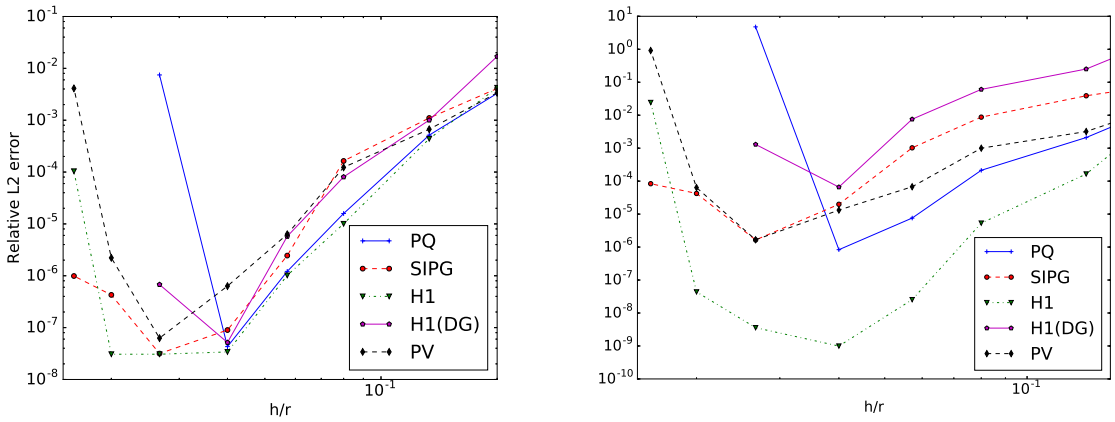

Figure 15: Relative L^2 error (left) and consistency error (right) versus h/r for coeff=0.2 and different formulations. Case of a non-uniform flow.

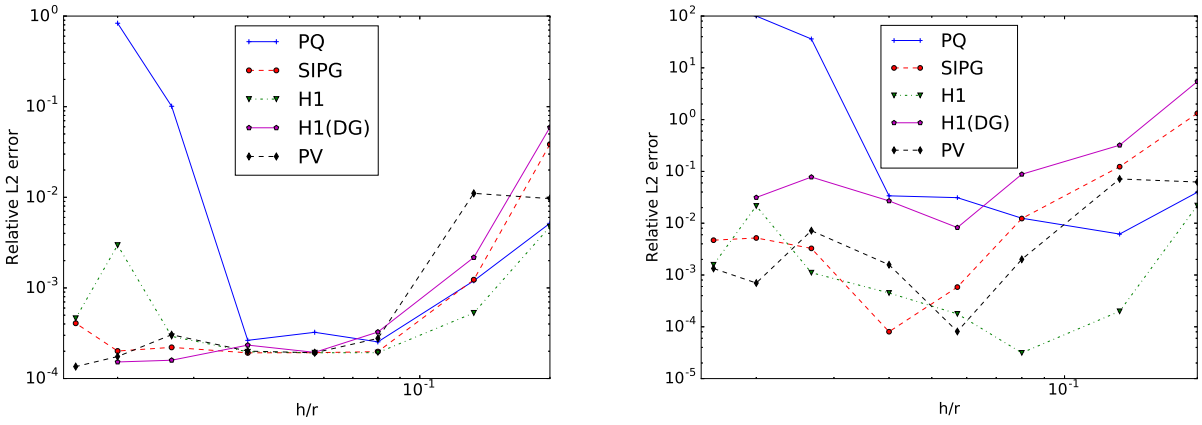

Figure 16: Relative L^2 error (left) and consistency error (right) versus h/r for coeff=0.5 and different formulations. Case of a non-uniform flow.

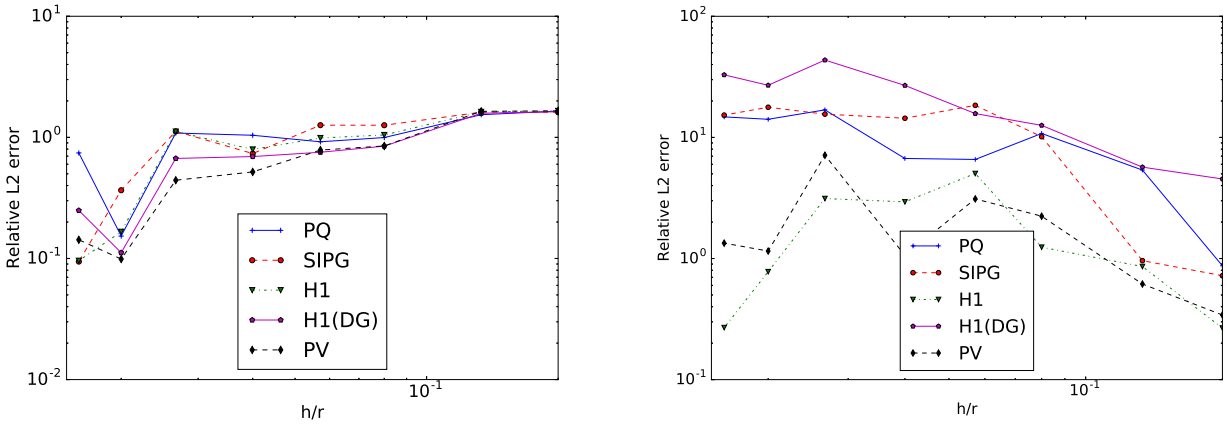

Figure 17: Relative L^2 error (left) and consistency error (right) versus h/r for coeff=1.5 and different formulations. Case of a non-uniform flow.

4 Stabilization of Galbrun's equation

4.1 Convergence for LEE

When Linearized Euler Equations (LEE) are solved (equation (2)) for a centered gaussian source g of radius equal to 1 (the same g as in subsection 3.2), we did not observe lack of convergence or robustness. In figure 18, we have displayed the relative L^2 error and consistency error (with adapted terms $S1$ and $S2$ for LEE) versus h/r for different values of coeff. The same periodic non-uniform flow has been chosen as for the previous section. The results have been obtained

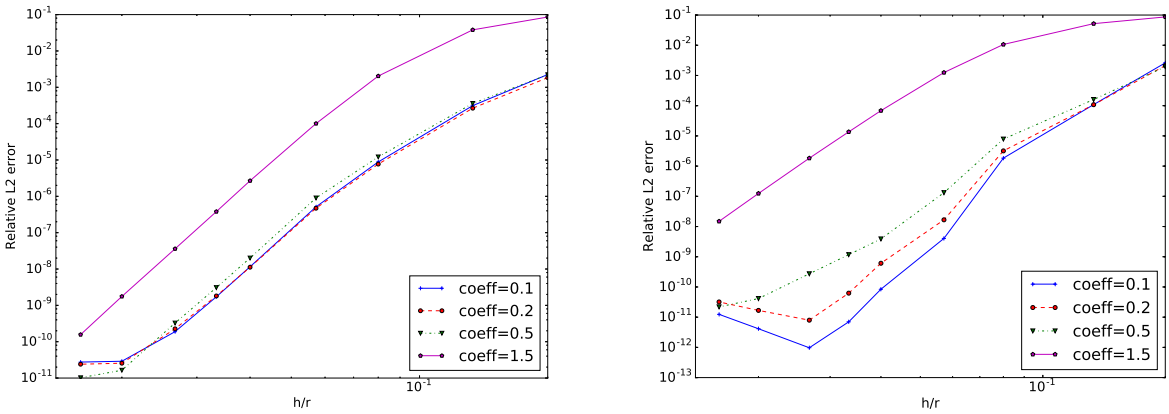

Figure 18: Relative L^2 error (left) and consistency error (right) versus h/r for different values of coeff and LEE. Case of a non-uniform flow.

with Discontinuous Galerkin method applied to LEE equations with upwind fluxes. A nice convergence is observed for any value of coeff. The solutions are displayed in figures 9, 10, 11, 12. For coeff=1.5, the solution is very nice compared to the solution obtained with Galbrun's equations.

4.2 Stabilized Galbrun's equation

When we tried to compute upwind fluxes for formulation PQ, we have noticed that the matrix B_n was not diagonalizable except in the two following cases

- the flow M is null
- the gradients $\nabla M, \nabla \rho_0, \nabla p_0$ are null

The eigenvalues of the matrix B_n are however real, thus providing a weakly hyperbolic system. Therefore, our approach was to investigate which terms could be dropped in the formulation (9) in order to obtain a diagonalizable B_n. The first approach consists of removing the flow part in

equation q:

$$\begin{cases} \rho_0 \left(-i\omega + \sigma + M \cdot \nabla\right) u - \nabla p - \rho_0 \, q = 0 \\ \rho_0 \left(-i\omega + \sigma\right) q - (\nabla\sigma) \, p - (\nabla M)^T \nabla p - \dfrac{M \cdot \nabla \rho_0}{\rho_0} \nabla p + (\operatorname{div} u) \nabla p_0 - (\nabla u)^T \nabla p_0 = f \\ \rho_0 \left(-i\omega + \sigma + M \cdot \nabla\right) p - \rho_0^2 \, c_0^2 \operatorname{div} u = 0 \end{cases} \tag{14}$$

These equations will be called Galbrun's equations with convective stabilization. For this stabilization procedure, it can be observed that the unknown q can be eliminated. The second approach consists of removing the non-uniform part in equation q :

$$\begin{cases} \rho_0 \left(-i\omega + \sigma + M \cdot \nabla\right) u - \nabla p - \rho_0 \, q = 0 \\ \rho_0 \left(-i\omega + \sigma + M \cdot \nabla\right) q - (\nabla\sigma) \, p = f \\ \rho_0 \left(-i\omega + \sigma + M \cdot \nabla\right) p - \rho_0^2 \, c_0^2 \operatorname{div} u = 0 \end{cases} \tag{15}$$

These equations will be called Galbrun's equations with non-uniform stabilization. For these two stabilized equations, the matrix B_n is diagonalizable with real eigenvalues. In figure 19, the

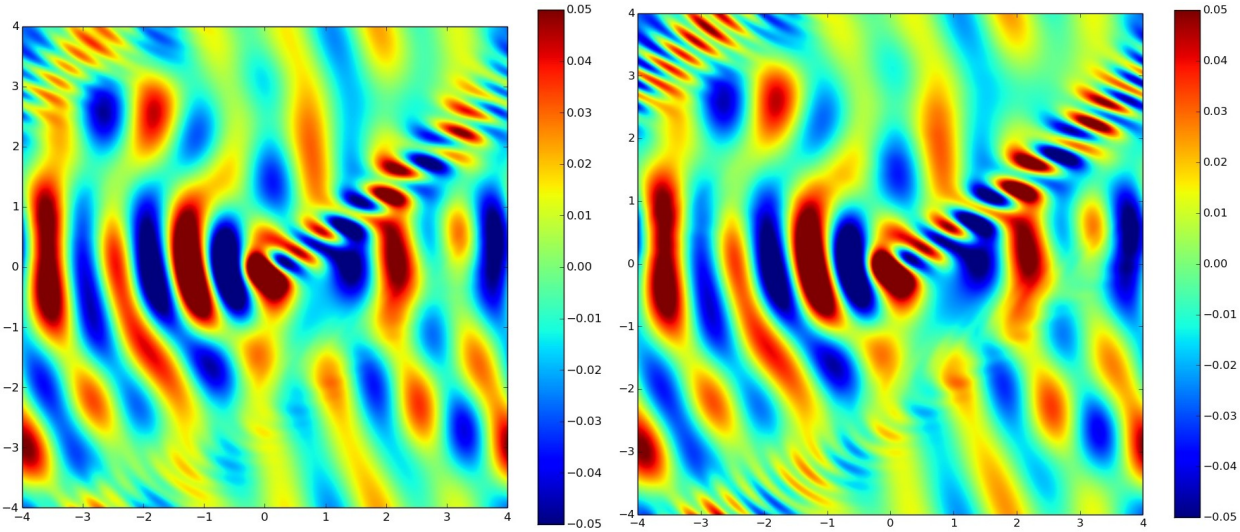

Figure 19: Real part of u_x for a non-uniform flow (coeff=1.5) and stabilized Galbrun's equations (on left, convective stabilization, on right non-uniform stabilization)

solution obtained for coeff=1.5 is displayed for the two kinds of stabilization. A nice convergence has been observed for any value of coeff (cf. figure 21 for coeff=1.5).

4.3 Simplified Galbrun's equations

A simplified Galbrun equation can be written by starting from formulation PQ, and neglecting the unknown q. Terms involving p_0 are added such that the simplified equations give the same solution as the original Galbrun's equation for a null flow and uniform damping σ. The simplified

Galbrun's equations are given as

$$\begin{cases} \rho_0(-i\omega + \sigma + M\cdot\nabla)\, p + \rho_0^2\, c_0^2\, \mathrm{div}\, u = 0 \\ \rho_0(-i\omega + \sigma + M\cdot\nabla)\, u + \nabla p + \dfrac{1}{-i\omega+\sigma}\left((\mathrm{div}\, u)\nabla p_0 - (\nabla u)^T \nabla p_0\right) = g \end{cases} \tag{16}$$

The solution obtained with simplified Galbrun's equation is displayed in figure 20. The relative

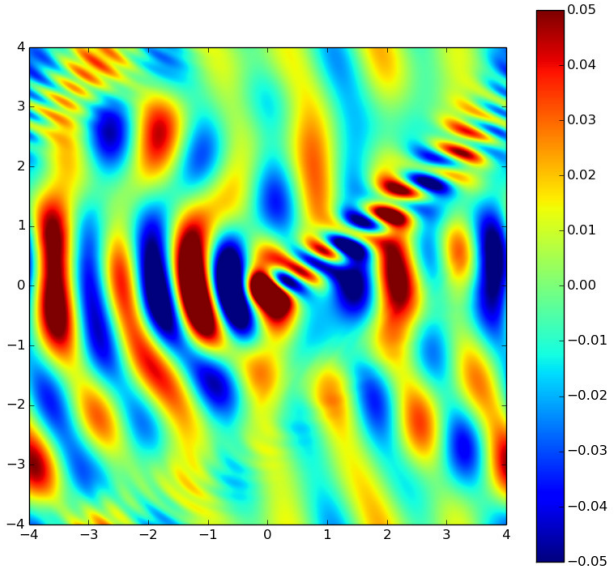

Figure 20: Real part of u_x for a non-uniform flow (coeff=1.5) and simplified Galbrun's equations

L^2 error (with respect to a reference solution computed with $\mathbb{Q}_{12}$ and 51 points) is represented versus h/r for the different approximate models presented here (convective stabilization, non-uniform stabilization, simplified Galbrun) in figure 21. Of course the reference solution differs for each model. For these three models, we observe that the numerical method converges quickly to the reference solution as expected.

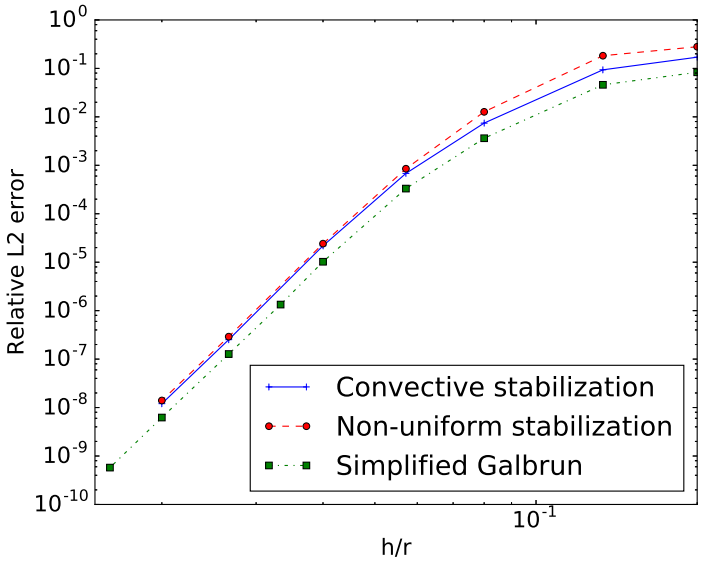

Figure 21: Relative L^2 error versus h/r for Galbrun's equations with convective stabilization, with non-uniform stabilization and simplified Galbrun's equations

5 Efficient computation of Green's function

In this section, only simplified Galbrun's equations (16) are considered since we are not able to compute the solution of original Galbrun's equations accurately. We consider a Dirac source, that is to say

$$g = \delta_{x=0}\, e_i$$

The polarization of the Dirac (vector e_i) can be chosen equal to e_x or e_y.

5.1 Null flow

When the flow M is null, the background uniform and the medium infinite, the analytical solution for unknown p and for the polarization e_x is given as

$$p = \frac{ik}{4}\frac{x}{\sqrt{x^2+y^2}} H_1^{(1)}\left(k\sqrt{x^2+y^2}\right)$$

where $H_n^{(1)}$ is the Hankel function of the first kind of order n. The wave number k is equal to

$$k = \frac{\omega + i\sigma}{c_0}$$

For the numerical experiments, we have chosen the following parameters

$$M = (0,0), \quad \rho_0 = 2.5, \quad c_0 = 0.8, \quad p_0 = 1, \quad \omega = 0.78 \times 2\,\pi, \quad \sigma = 0.1$$

The computational domain is the square $[-4,4]$ surrounded by PML layers. For PML layers, they are implemented classically with a complex change of coordinates

$$\widetilde{x} = x + \frac{i}{\omega}\int_{x_0}^{x} \sigma(s) ds$$

where x_0 is the starting position of the PML and the damping σ is parabolic

$$\sigma(s) \;=\; \frac{3\,\log(R)}{2a^3}(s-x_0)^2\, c_0$$

the coefficient R is here taken equal to 10^{12} to have a neglegible reflection from PML. We are using classical PMLs which are not adapted for Galbrun's equations (see e.g. [8], [12] for adapted PMLs) but as pointed out in [12], classical PMLs work quite well in time-harmonic domain as far as the damping is large enough (which is our case). In figure 22, the numerical solution is displayed (and the mesh used to obtain it). We observed that the solution is incorrect in the vicinity of the origin (where the Dirac is centered). In order to obtain a correct solution, a local refinement must be applied. In figure 23, the result is displayed when the mesh is locally refined at the center. The solution still remains incorrect for elements close to the center of the Dirac. However, since they are very small, it is hardly noticeable. In figure 24, we have computed the relative L^2 error between the numerical solution and the analytical solution (for unknown p only) on the computational domain stripped of the disk of radius 1 centered at the origin. This disk is excluded in order to not take into account the elements close to the origin where the solution is incorrect. We observe that the numerical solution converges nicely to the analytical one, especially when a local refinement is applied.

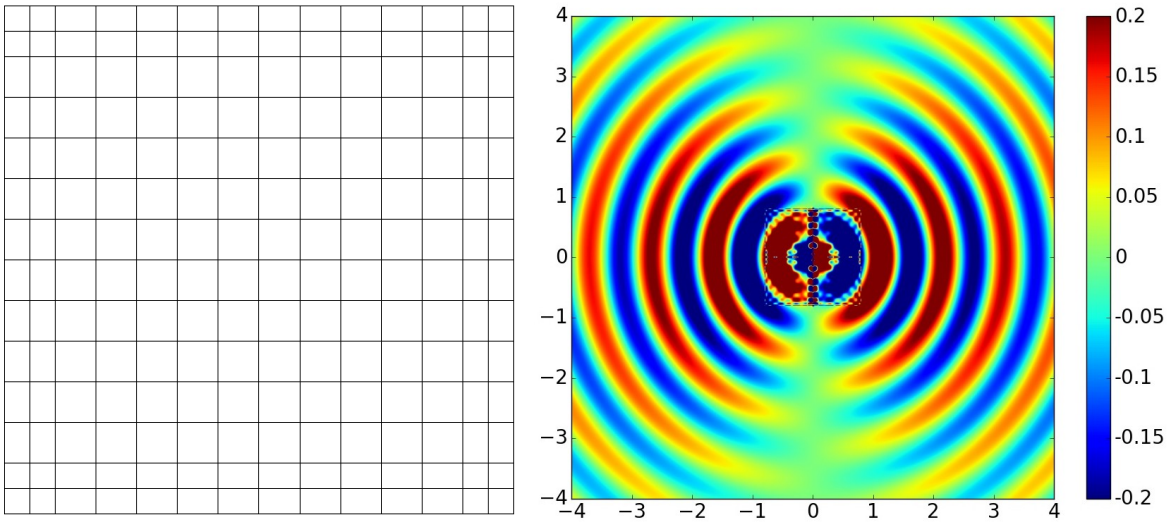

Figure 22: At left mesh used to obtain the numerical solution (real part of p) displayed at right. Case of a null flow, $\mathbb{Q}_{10}$ finite element is used.

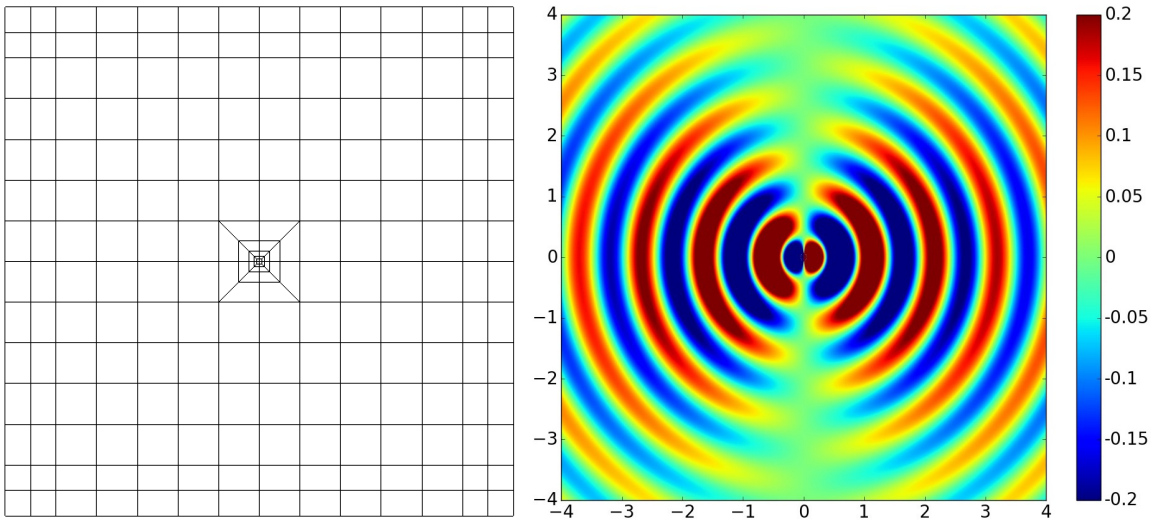

Figure 23: At left mesh used to obtain the numerical solution (real part of p) displayed at right. Case of a null flow, $\mathbb{Q}_{10}$ finite element is used.

5.2 Uniform flow

We now choose an uniform flow with the following parameters

$$M = (0, 0.3), \quad \rho_0 = 2.5, \quad c_0 = 0.8, \quad p_0 = 1, \quad \omega = 0.78 \times 2\,\pi, \quad \sigma = 0.1$$

The Dirac is polarized along e_y, the solution obtained is displayed in figure 25 for a mesh locally refined (as in figure 23) for two types of numerical fluxes (Discontinuous Galerkin formulation is

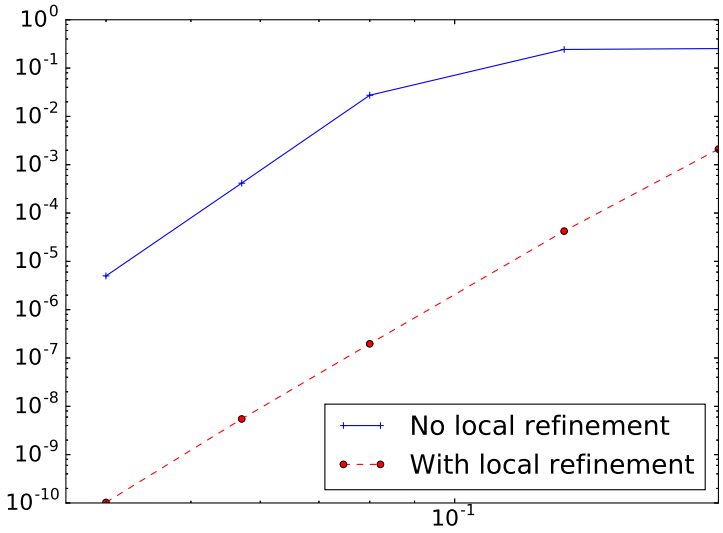

Figure 24: Relative L^2 error for a Dirac source with a null flow versus h/r.

used). Upwind fluxes have already been detailed previously, the penalty matrix is given as

$$P(x) = |B_n|$$

Acoustical upwind fluxes consist of choosing the penalty matrix by considering that the flow is equal to 0 :

$$P(x) = |B_n|_{M=0}$$

Figure 25 shows that choosing upwind fluxes avoids the propagation of undesired oscillations in the opposite direction of the flow. However, the vortex wave that propagates at the velocity M is not correctly resolved since the mesh should be refined along the path of this vortex wave. In figure 26, the solution is displayed for a mesh which is refined towards the axis Oy such that the vortex wave is correctly captured.

5.3 Non-Uniform flow

For a non-uniform, the mesh should be refined along the path of the vortex wave which follows the flow. In figure 27, we have displayed the numerical solution computed on a regular mesh locally refined at the origin for a Dirac source with the polarization e_y. Since it is not refined along this path, undesired oscillations appear in the numerical solution both for unknowns p and u_y. We have chosen the non-uniform flow defined in subsection 3.2 with coeff=0.5. The computational domain is truncated with zero-order absorbing boundary condition described in appendix A. We have used $\mathbb{Q}_{10}$ finite element with $N = 31$ points in x and y.

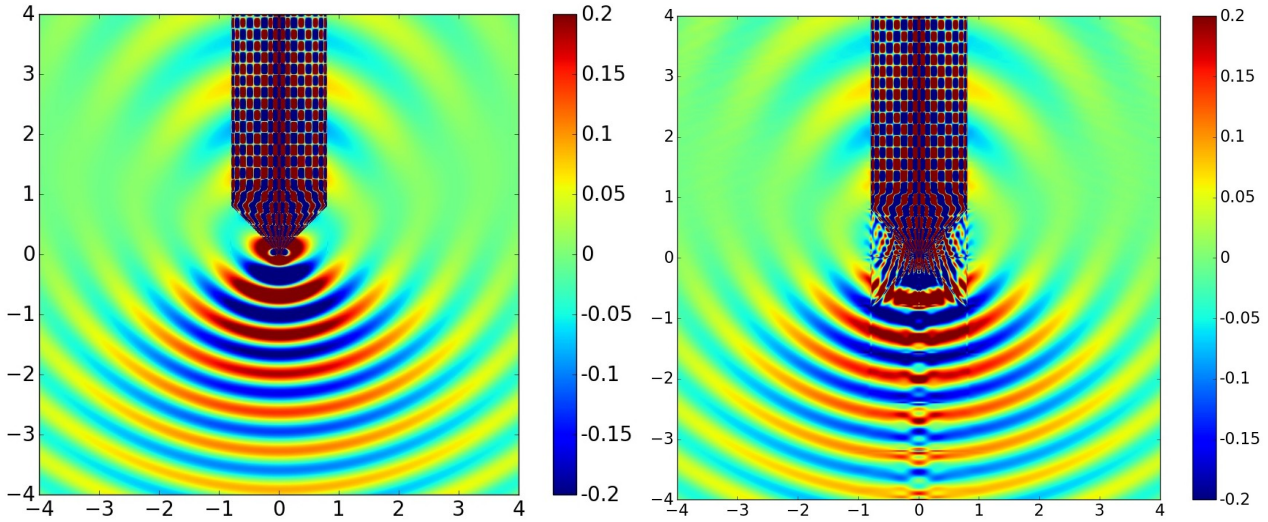

Figure 25: Real part of u_y for a Dirac source and an uniform flow. At left, upwind fluxes are chosen, at right acoustical upwind fluxes.

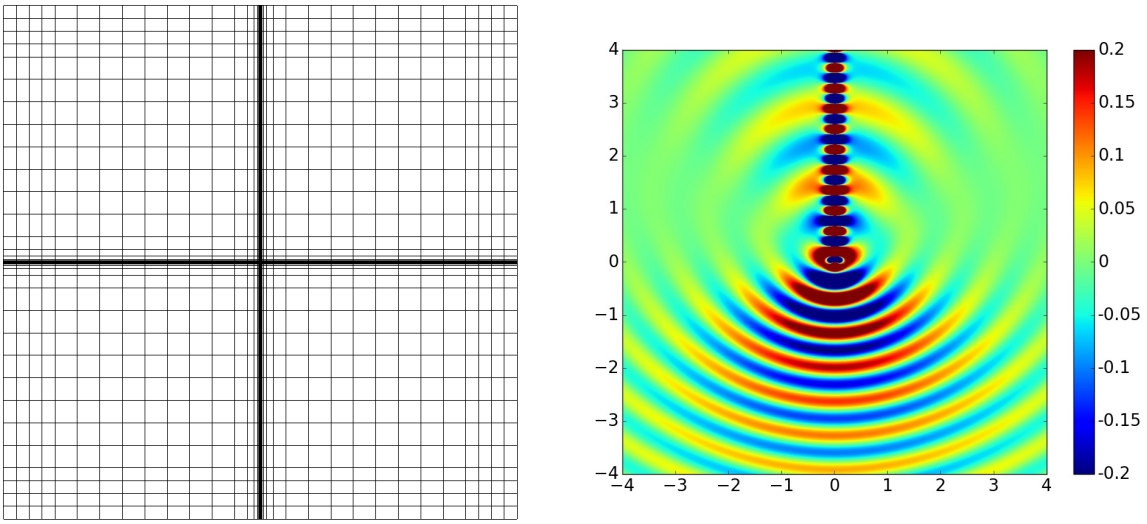

Figure 26: At left, mesh used to obtain the numerical solution on the right (real part of u_y). Case of an uniform flow, $\mathbb{Q}_{10}$ finite element is used.

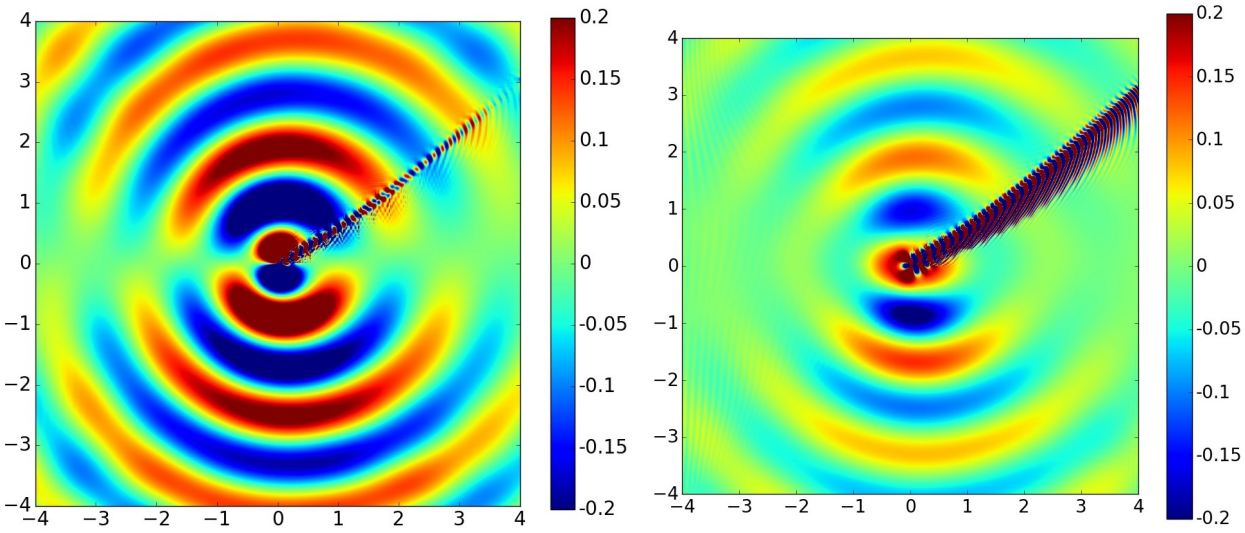

Figure 27: Real part of p (left) and u_y (right) for a Dirac source and non-uniform flow.

6 Numerical results for the Sun

In this section, numerical experiments are conducted for the sun which is assumed to be a perfect ball. The coefficients ρ_0, c_0 and p_0 are directly provided for different radii r_i with realistic values of the sun (cf. the model S of [7]). In figure 28, the sound speed and density are plotted with respect to the relative radius (close to 0 is the center of the Sun, close to 1 is the surface). The values for any r are then obtained by a cubic spline interpolation, such that the coefficients are C^2-continuous. We take the following parameters

$$\omega = 2\pi f, \quad \sigma = \frac{\omega}{100}$$

The frequency f is chosen as 3 mHz. An adimensionalization is performed such that this frequency (and σ) are multiplied by the radius of the sun (equal to $7 \cdot 10^8$ m) and a ball of radius 1.0007126 is considered. In this section, $\mathbb{Q}_{10}$ finite elements are used in conjunction with upwind

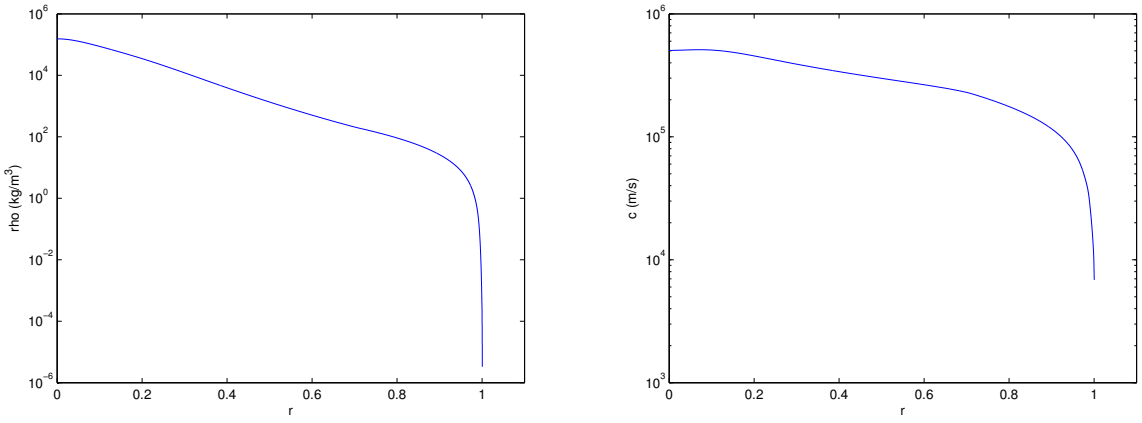

Figure 28: On the left: density ρ versus the radius r, on the right: sound speed c.

fluxes. For the solution of Galbrun's equations, the formulation PQ is chosen.

6.1 2-D results

In this subsection, the computations are performed in 2-D, the sun is a perfect disk. The flow M is chosen equal to

$$M = \frac{\text{coeff}}{R} c_0(r) \begin{bmatrix} -y \\ x \end{bmatrix}$$

where R is the radius of the sun (almost 1 with our adimensionalization) and coeff a coefficient that will depend on the experiment. The mesh used for the simulations is adapted to the sun (mainly to variations of ρ_0 and c_0, see figure 29). The source g is a gaussian located at the point

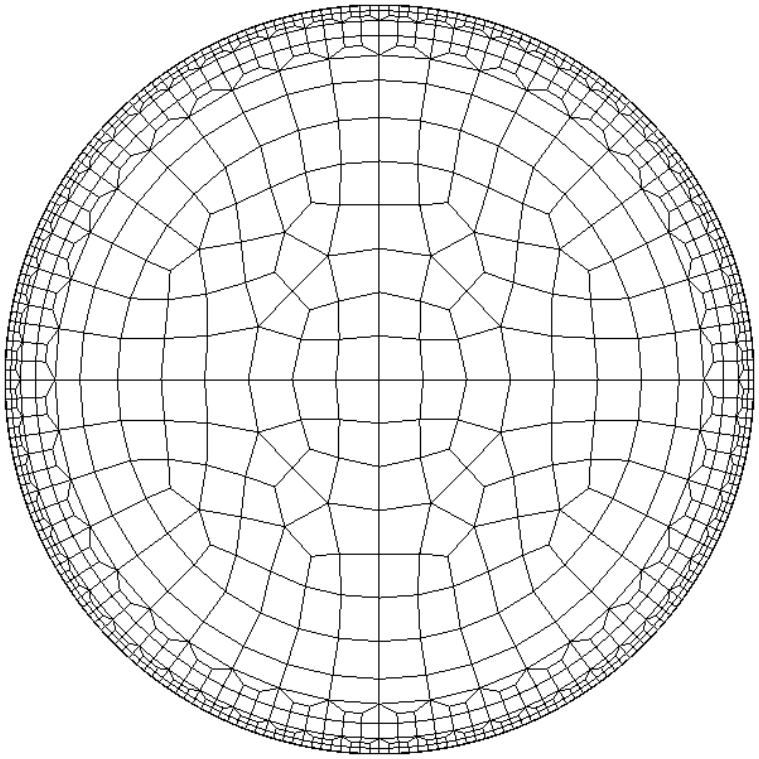

Figure 29: Mesh used for 2-D experiments

$(0.5, 0.5)$ with a radius of distribution equal to 0.1 and polarized in x direction. The source f satisfies the relation :

$$f \;=\; (-i\omega + \sigma + M \cdot \nabla)g$$

A Neumann boundary condition is set on the external circle :

$$\operatorname{div} u = 0$$

In figure 30, the displacement u_x is displayed when the sun is quiet (coeff=0) for Galbrun's equations and LEE. We see that the solutions differ, but they are accurately computed for these two kinds of equations. Because of this difference, simplified Galbrun's equations are preferred. In figure 31, the solution for Galbrun's equations and simplified Galbrun's equations are displayed for coeff = 0.2. It can be noted that the two solutions seem similar. In figure 32, the two solutions are represented for a transsonic flow (since the magnitude of M is equal to c_0 at the surface of the sun). Simplified Galbrun's equations provide a realistic solution contrary to the original Galbrun's equations which are polluted by undesired oscillations.

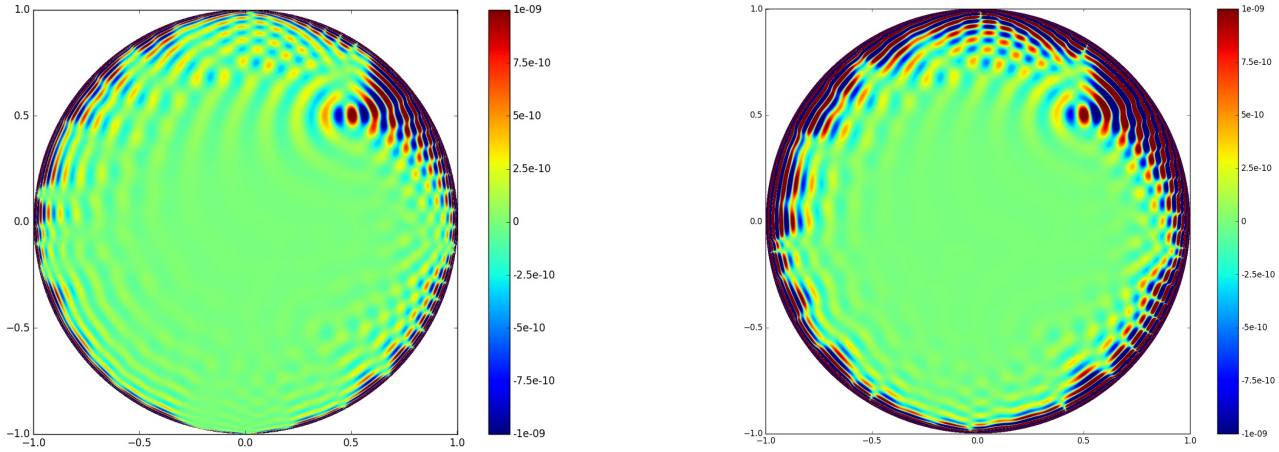

Figure 30: Real part of u_x for Galbrun's equations (left) and u_x/ρ_0 for Linearized Euler's equations (right). Case of a quiet sun (coeff=0).

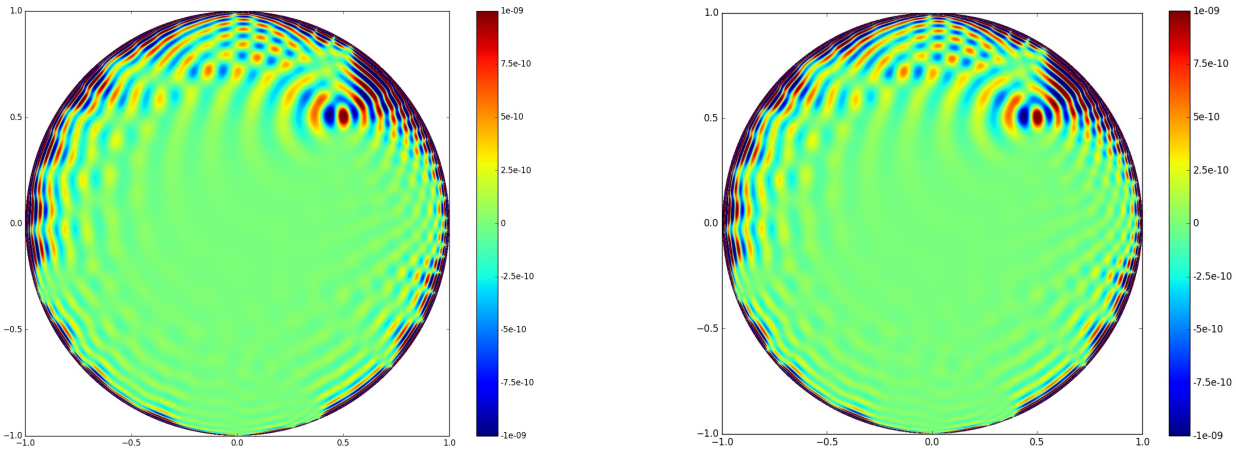

Figure 31: Real part of u_x for Galbrun's equations (left) and simplified Galbrun's equations (right). Case of a subsonic flow (coeff=0.2).

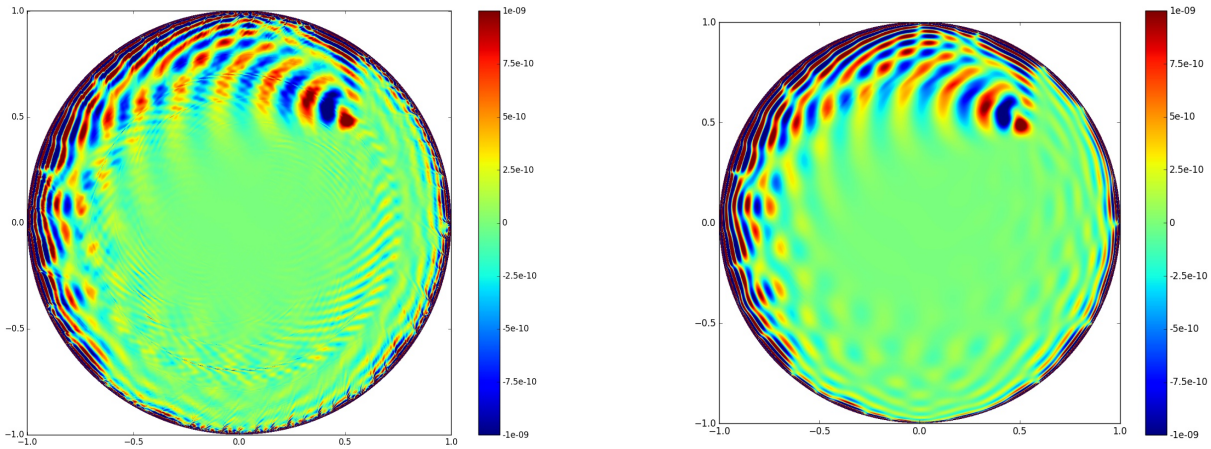

Figure 32: Real part of u_x for Galbrun's equations (left) and simplified Galbrun's equations (right). Case of a transsonic flow (coeff=1.0).

6.2 Axisymmetric results

In this subsection, the computations are performed in 3-D, the surface of the sun is a sphere. Since the geometry is axisymmetric, the computations can be performed in 2.5-D, only a half-disk is used to represent the section of the geometry in (r, z) plane. In the appendix C, it is explained how computations are lead in 2-D whereas the geometry is 3-D by using cylindrical coordinates (r, θ, z) and decomposing the solution in its Fourier modes in θ. The problems encountered in 2-D for the solution of original Galbrun's equations are also observed in the axisymmetric case. The source g is a gaussian located at the point $(0.0, 0.7)$ with a radius of distribution equal to 0.2 and polarized in x direction. The source f satisfies the relation :

$$f \;=\; (-i\omega + \sigma + M \cdot \nabla) g$$

A Neumann boundary condition is set on the external circle :

$$\operatorname{div} u = 0$$

Since the center of the gaussian belongs to the axis Oz, only Fourier modes $m = \pm 1$ are needed to obtain the solution in 3-D. In figure 33, the solution obtained for Galbrun's equations and

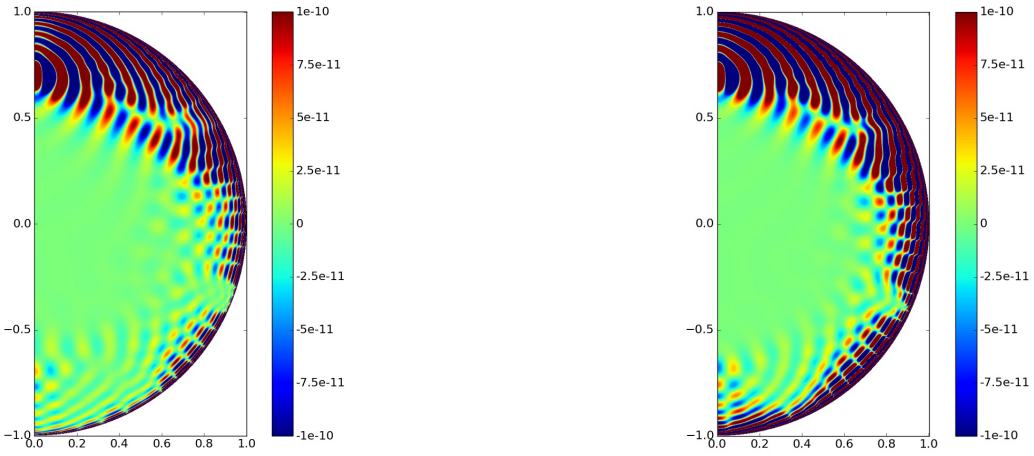

Figure 33: Real part of u_x for Galbrun's equations (left) and u_x/ρ_0 for Linearized Euler's equations (right) in plane Oxz. Case of a quiet sun (C=0).

LEE are plotted for a quiet sun ($M = 0$). For a non-quiet sun, we choose a meridional flow

$$\begin{aligned} M \;=\; & \left[u_s(r) \sin\theta \; P_s(\cos\theta) - v_s(r) \sin\theta \cos\theta \; P_s'(\cos\theta)\right] u_r \\ & + \left[u_s(r) \cos\theta \; P_s(\cos\theta) + v_s(r) \sin^2\theta \; P_s'(\cos\theta)\right] u_z \end{aligned}$$

where

$$u_s(r) = \begin{cases} \mathrm{C}\, c_0(r)\, \rho_0(r) \dfrac{(r - r_b)^2 (r_t - r)^2}{0.0005}, & \text{if } r_b \le r \le r_t \\ 0 \text{ otherwise} \end{cases}$$

$$v_s(r) = \frac{ru_s'(r) + 2u_s(r)}{s(s+1)}$$

in cylindrical coordinates where P_s are Legendre polynomials. We have chosen the following numerical values:

$$s = 1, \quad r_b = 0.7, \quad r_t = 0.984788$$

The divergence of M is null, but the divergence of $\rho_0 M$ is non-null. In figures 34 and 35, the solution is computed respectively for C $= 10^{-3}$ and C $= 3 \cdot 10^{-3}$ for Galbrun's equations and simplified Galbrun's equations. We see instabilities appearing when solving original Galbrun's equations, whereas the simplified version gives nice results.

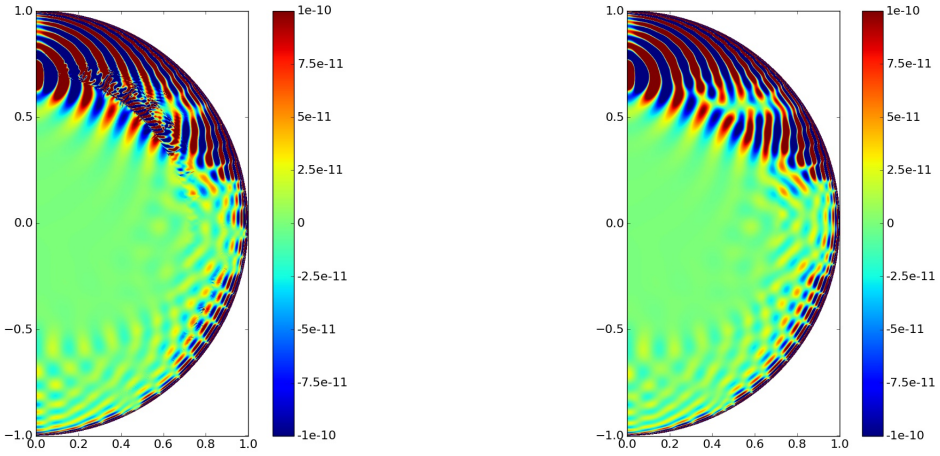

Figure 34: Real part of u_x for Galbrun's equations (left) and simplified Galbrun's equations (right) in plane Oxz. Case of a meridional flow (C=1e-3)).

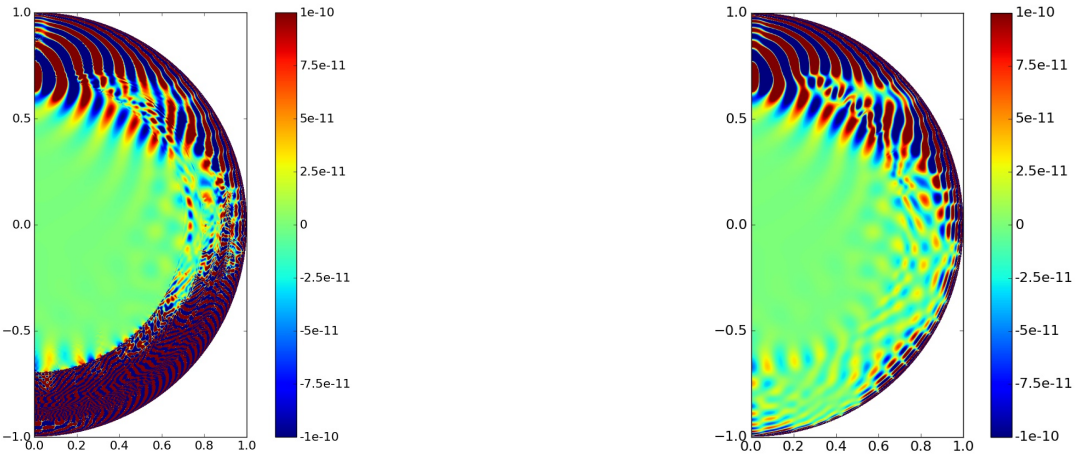

Figure 35: Real part of u_x for Galbrun's equations (left) and simplified Galbrun's equations (right) in plane Oxz. Case of a meridional flow (C=3e-3)).

References

[1] P.R. Amestoy, I.S. Duff, J. Koster, and J.-Y. L'Excellent. A fully asynchronous multifrontal solver using distributed dynamic scheduling. *SIAM Journal on Matrix Analysis and Applications*, 23:15–41, 2001.

[2] M. Bernacki. *Méthodes de type Galerkin discontinu pour la propagation des ondes en aéroacoustique.* PhD thesis, Ecole Nationale des Ponts et Chaussées, 2005.

[3] C. Bogey, C. Bailly, and D. Juve. Computation of flow noise using source terms in linearized Euler's equations. *AIAA Journal*, 40(2):225–243, 2002.

[4] Anne-Sophie Bonnet-BenDhia, Jean-François Mercier, Florence Millot, and Sébastien Pernet. A low mach model for time harmonic acoustics in arbitrary flows. *Journal of Computational and Applied Mathematics*, 234(6):1868–1875, 2010.

[5] Anne-Sophie Bonnet-BenDhia, Jean-François Mercier, Florence Millot, Sébastien Pernet, and Emilie Peynaud. Time-harmonic acoustic scattering in a complex flow: a full coupling between acoustics and hydrodynamics. *Communications in Computational Physics*, 11(2):555–572, 2 2012.

[6] M. Duruflé. *Intégration numérique et éléments finis d'ordre élevé appliqués aux équations de Maxwell en régime harmonique.* PhD thesis, Université Paris IX-Dauphine, 2006.

[7] Christensen-Dalsgaard et al. The current state of solar modeling. *Science*, 272:1286–1292, 1996.

[8] Xue Feng. *Modélisation numérique par éléments finis d'un problème aéroacoustique en régime transitoire : application à l'équation de Galbrun.* PhD thesis, Université de Technologie de Compiègne, 2013.

[9] H. Galbrun. *Propagation d'une onde sonore dans l'atmosphère terrestre et théorie des zones de silence.* Gauthier-Villars, Paris, France, 1931.

[10] Marcus Grote, Anna Scheebeli, and Dominik Schötzau. Discontinuous Galerkin finite element method for the wave equation. *SIAM J. Num. Analysis*, 44:2408–2431, 2006.

[11] J.S. Hesthaven and T. Warburton. Nodal high-order methods on unstructured grids. *Journal of Computational Physics*, 181:186–221, 2002.

[12] Guillaume Legendre. *Rayonnement acoustique dans un fluide en écoulement : Analyse mathématique et numérique de l'équation de Galbrun.* PhD thesis, Université Pierre et Marie Curie, 2003.

[13] D. Lynden-Bell and J.P. Ostriker. On the stability of differentially rotating bodies. *Mon. Not. R. astr. Soc.*, 136:293–310, 1967.

A Zero-order absorbing boundary condition for linear hyperbolic systems

A.1 Transparent condition

In this section, we consider an hyperbolic system of the form:

$$M\frac{\partial U}{\partial t} + A_x\frac{\partial U}{\partial x} + A_y\frac{\partial U}{\partial y} + A_z\frac{\partial U}{\partial z} + CU = 0$$

This equation is solved in the half-space $z < 0$, we want to find an absorbing boundary condition on the plane $z = 0$ such that outgoing waves are not reflected. An outgoing plane wave is given as:

$$U = \hat{U}e^{i(k_x x + k_y y + k_z z) - i\omega t}$$

where $k_z > 0$. A negative k_z would correspond to an ingoing plane wave. We obtain:

$$(-i\omega M + ik_x A_x + ik_y A_y + ik_z A_z + C)\hat{U} = 0$$

A non-trivial solution of this system is obtained if k_z solves the following eigenvalue problem:

$$(\omega M - k_x A_x - k_y A_y + iC)\hat{U} = k_z A_z \hat{U}$$

which is rewritten as

$$A_z\hat{U} = \lambda\left(M - \frac{k_x}{\omega}A_x - \frac{k_y}{\omega}A_y + \frac{i}{\omega}C\right)\hat{U}$$

where the eigenvalues are equal to

$$\lambda = \frac{\omega}{k_z}$$

Outgoing waves are eigenvectors associated with this system, such that $k_z > 0$. Let us denote:

$$\widetilde{M} = \left(M - \frac{k_x}{\omega}A_x - \frac{k_y}{\omega}A_y + \frac{i}{\omega}C\right)$$

If we note V the basis of the eigenvectors associated with this problem, we have:

$$A_z = \widetilde{M}VLV^{-1}$$

The positive, negative and absolute value of A_z is defined through these eigenvectors V:

$$A_z^- = \widetilde{M}VL^-V^{-1}, \quad A_z^+ = \widetilde{M}VL^+V^{-1}, \quad |A_z| = \widetilde{M}V|L|V^{-1}$$

A solution that consists only of outgoing waves, satisfy:

$$A_z^-\hat{U} = 0$$

this equality can be written also as:

$$A_z\hat{U} = |A_z|\hat{U}$$

This condition is a transparent condition, but is non-local since Fourier transforms in (x, y) are needed. For a general plane whose normale is $n = (n_x, n_y, n_z)$, we denote the matrix D as:

$$D = n_x A_x + n_y A_y + n_z A_z$$

For this matrix D, negative, positive and absolute value are defined as for A_z, the transparent condition is given as:

$$D\hat{U} = |D|\hat{U}$$

A.2 Zero-order approximation

In this approximation, only M term is kept, this approximation is valid if M is invertible. The eigenvalue problem is given as:

$$D\hat{U} = \lambda M\hat{U}$$

Once the eigenvectors are computed, $|D|$ can be computed, and the zero-order absorbing boundary condition is equal to:

$$DU = |D|U$$

A.3 Expressions for LEE

A.3.1 Simplified model and Bogey-Bailly-Juve model

For these models, we have

$$M = I, \quad D = \begin{pmatrix} \alpha & c_0^2 n^T \\ n & \alpha\, I \end{pmatrix}$$

where $\alpha = \vec{M}\cdot n$, $\vec{M}$ being the flow on the boundary. The eigenvalues and eigenvectors are given as (in 2-D):

$$L = \begin{pmatrix} \alpha \\ \alpha + c_0 \\ \alpha - c_0 \end{pmatrix}, \quad V = \begin{pmatrix} 0 & c_0 & -c_0 \\ -n_y & n_x & n_x \\ n_x & n_y & n_y \end{pmatrix}, V^{-1} = \begin{pmatrix} 0 & -n_y & n_x \\ \dfrac{1}{2c_0} & \dfrac{n_x}{2} & \dfrac{n_y}{2} \\ -\dfrac{1}{2c_0} & \dfrac{n_x}{2} & \dfrac{n_y}{2} \end{pmatrix}$$

The absolute value of D is equal to:

$$|D| = \begin{pmatrix} s & d\, c_0\, n^T \\ \dfrac{d\, n}{c_0} & |\alpha| I + (s - |\alpha|)\, n\, n^T \end{pmatrix}$$

where

$$s = \frac{1}{2}\left(|\alpha + c_0| + |\alpha - c_0|\right), \quad d = \frac{1}{2}\left(|\alpha + c_0| - |\alpha - c_0|\right)$$

A.3.2 Linearized Euler Equations

We have

$$M = I, \quad D = \begin{pmatrix} \alpha & 0 & c_0^2 n^T \\ 0 & \alpha & n^T \\ n & 0 & \alpha I \end{pmatrix}$$

where $\alpha = \vec{M}\cdot n$, $\vec{M}$ being the flow on the boundary. The eigenvalues and eigenvectors are given as (in 2-D):

$$L = \begin{pmatrix} \alpha \\ \alpha \\ \alpha + c_0 \\ \alpha - c_0 \end{pmatrix}, \quad V = \begin{pmatrix} 0 & 0 & c_0 & -c_0 \\ -1 & 1 & \dfrac{1}{c_0} & -\dfrac{1}{c_0} \\ -n_y & -n_y & n_x & n_x \\ n_x & n_x & n_y & n_y \end{pmatrix}, V^{-1} = \begin{pmatrix} \dfrac{1}{2c_0^2} & -\dfrac{1}{2} & -\dfrac{n_y}{2} & \dfrac{n_x}{2} \\ -\dfrac{1}{2c_0^2} & \dfrac{1}{2} & -\dfrac{n_y}{2} & \dfrac{n_x}{2} \\ \dfrac{1}{2c_0} & 0 & \dfrac{n_x}{2} & \dfrac{n_y}{2} \\ -\dfrac{1}{2c_0} & 0 & \dfrac{n_x}{2} & \dfrac{n_y}{2} \end{pmatrix}$$

The absolute value of D is equal to:

$$|D| = \begin{pmatrix} s & 0 & d\,c_0\,n^T \\ \dfrac{s-|\alpha|}{c_0^2} & |\alpha| & \dfrac{d}{c_0}\,n^T \\ \dfrac{d\,n}{c_0} & 0 & |\alpha| I + (s-|\alpha|)\,n\,n^T \end{pmatrix}$$

where

$$s = \frac{1}{2}\left(|\alpha + c_0| + |\alpha - c_0|\right), \quad d = \frac{1}{2}\left(|\alpha + c_0| - |\alpha - c_0|\right)$$

A.4 Galbrun's equations

For the formulation PQ, we have (in 2-D) :

$$M = \rho_0 I, \quad D = \begin{pmatrix} \rho_0\alpha & 0 & 0 & 0 & -n_x \\ 0 & \rho_0\alpha & 0 & 0 & -n_y \\ 0 & \rho_0\gamma & \rho_0\alpha & 0 & \beta_x \\ -\rho_0\gamma & 0 & 0 & \rho_0\alpha & \beta_y \\ -(\rho_0 c_0)^2 n_x & -(\rho_0 c_0)^2 n_y & 0 & 0 & \rho_0\alpha \end{pmatrix}$$

where

$$\alpha = \vec{M}\cdot n, \quad \rho_0\gamma = \nabla p_0 \times n$$

$$(\beta_x, \beta_y) = (-\nabla M)^T\, n - \frac{M\cdot\nabla\rho_0}{\rho_0} n$$

For an uniform flow, we have

$$\gamma = \beta_x = \beta_y = 0$$

In this case, the eigenvalues and eigenvectors are given as :

$$L = \begin{pmatrix} \alpha \\ \alpha \\ \alpha \\ \alpha + c_0 \\ \alpha - c_0 \end{pmatrix}$$

$$V = \begin{pmatrix} -n_y & 0 & 0 & -n_x & n_x \\ n_x & 0 & 0 & -n_y & n_y \\ 0 & 1 & 0 & 0 & 0 \\ 0 & 0 & 1 & 0 & 0 \\ 0 & 0 & 0 & \rho_0 c_0 & \rho_0 c_0 \end{pmatrix}, V^{-1} = \begin{pmatrix} -n_y & n_x & 0 & 0 & 0 \\ 0 & 0 & 1 & 0 & 0 \\ 0 & 0 & 0 & 1 & 0 \\ \dfrac{-n_x}{2} & \dfrac{-n_y}{2} & 0 & 0 & \dfrac{1}{2\rho_0 c_0} \\ \dfrac{n_x}{2} & \dfrac{n_y}{2} & 0 & 0 & \dfrac{1}{2\rho_0 c_0} \end{pmatrix}$$

The absolute value of D is equal to:

$$|D| = \rho_0 \begin{pmatrix} |\alpha| I + (s-|\alpha|)\,n\,n^T & 0 & -\dfrac{d}{\rho_0 c_0} n \\ 0 & |\alpha| I & 0 \\ -\rho_0 c_0\, d n^T & 0 & s \end{pmatrix}$$

where

$$s = \frac{1}{2}\left(|\alpha + c_0| + |\alpha - c_0|\right), \quad d = \frac{1}{2}\left(|\alpha + c_0| - |\alpha - c_0|\right)$$

For a non-uniform flow ($\gamma \neq 0$), the eigenvalue problems reads (assuming $\rho_0 = 1$ for sake of simplicity)

$$\left\{\begin{array}{l} \text{Find } \lambda, (x, y, u, v, p) \neq 0 \text{ such that} \\ (\lambda - \alpha)x = -n_x p \\ (\lambda - \alpha)y = -n_y p \\ (\lambda - \alpha)u = \gamma y + \beta_x p \\ (\lambda - \alpha)v = -\gamma x + \beta_y p \\ (\lambda - \alpha)p = -c_0^2(n_x x + n_y y) \end{array}\right.$$

If $\lambda = \alpha$, the two first equations give $p = 0$. Since $\gamma \neq 0$, the two following equations give $x = y = 0$. As a result, α is a double eigenvalue with eigenvectors $(0, 0, 1, 0, 0)$ and $(0, 0, 0, 1, 0)$. If $\lambda \neq \alpha$, the last equation multiplied by $(\lambda - \alpha)$ provides (x and y are substituted by using the two first equations):

$$(\lambda - \alpha)^2 p = c_0^2 p$$

If $p = 0$, we obtain the trivial solution $x = y = u = v = 0$. Therefore p is different from 0, and we obtain two simple eigenvalues :

$$\lambda = \alpha + c_0, \quad \text{eigenvector} = (-n_x c_0, -n_y c_0, -n_y\gamma + c_0\beta_x, n_x\gamma + c_0\beta_y, c_0^2)$$

$$\lambda = \alpha - c_0, \quad \text{eigenvector} = (n_x c_0, n_y c_0, -n_y\gamma - c_0\beta_x, n_x\gamma - c_0\beta_y, c_0^2)$$

Hence, only three eigenvalues of total multiplicity four exist whereas the matrix contains five rows. As a result, the system is not diagonalizable. The two proposed stabilizations are designed such that the new system is diagonalizable. For a non-uniform stabilization, the terms γ, β_x, β_y are dropped, providing the eigenvalues of the system for an uniform flow. For a convective stabilization, terms α are dropped in the diagonal, leading to the following system :

$$M = \rho_0 I, \quad D = \begin{pmatrix} \rho_0\alpha & 0 & 0 & 0 & -n_x \\ 0 & \rho_0\alpha & 0 & 0 & -n_y \\ 0 & \rho_0\gamma & 0 & 0 & \beta_x \\ -\rho_0\gamma & 0 & 0 & 0 & \beta_y \\ -(\rho_0 c_0)^2 n_x & -(\rho_0 c_0)^2 n_y & 0 & 0 & \rho_0\alpha \end{pmatrix}$$

The eigenvalues and eigenvectors of this system are given as

$$L = \begin{pmatrix} \alpha \\ 0 \\ 0 \\ \alpha + c_0 \\ \alpha - c0 \end{pmatrix}, \quad V = \begin{pmatrix} -n_y\alpha & 0 & 0 & -n_x & n_x \\ n_x\alpha & 0 & 0 & -n_y & n_y \\ \gamma n_x & 1 & 0 & \dfrac{-\gamma n_y + \beta_x c_0}{\alpha + c_0} & \dfrac{\gamma n_y + \beta_x c_0}{\alpha - c_0} \\ \gamma n_y & 0 & 1 & \dfrac{\gamma n_x + \beta_y c_0}{\alpha + c_0} & \dfrac{-\gamma n_x + \beta_y c_0}{\alpha - c_0} \\ 0 & 0 & 0 & c_0\rho_0 & c_0\rho_0 \end{pmatrix},$$

$$V^{-1} = \begin{pmatrix} \dfrac{-n_y}{\alpha} & \dfrac{n_x}{\alpha} & 0 & 0 & 0 \\ \times & \times & \times & \times & \times \\ \times & \times & \times & \times & \times \\ -\dfrac{n_x}{2} & -\dfrac{n_y}{2} & 0 & 0 & \dfrac{1}{2c_0\rho_0} \\ \dfrac{n_x}{2} & \dfrac{n_y}{2} & 0 & 0 & \dfrac{1}{2c_0\rho_0} \end{pmatrix}$$

The absolute value of D is equal to (in 2-D) :

$$|D| = \rho_0 \begin{pmatrix} |\alpha| + n_x^2(s-|\alpha) & n_x n_y(s-|\alpha|) & 0 & 0 & -\dfrac{n_x d}{\rho_0 c_0} \\ n_x n_y(s-|\alpha|) & |\alpha| + n_y^2(s-|\alpha) & 0 & 0 & -\dfrac{n_y d}{\rho_0 c_0} \\ n_x n_y \gamma(-s_a + s_\alpha) - n_x \beta_x c_0 d_\alpha & \gamma(s_a n_x^2 + s_\alpha n_y^2) - \beta_x n_y c_0 d_\alpha & 0 & 0 & -\dfrac{\gamma}{\rho_0 c_0} n_y d_\alpha + \dfrac{\beta_x}{\rho_0} s_\alpha \\ -\gamma(s_\alpha n_x^2 + s_a n_y^2) - \beta_y n_x c_0 d_\alpha & n_x n_y \gamma(s_a - s_\alpha) - \beta_y n_y c_0 d_\alpha & 0 & 0 & \dfrac{\gamma}{\rho_0 c_0} n_x d_\alpha + \dfrac{\beta_y}{\rho_0} s_\alpha \\ -n_x d \rho_0 c_0 & -n_y d \rho_0 c_0 & 0 & 0 & s \end{pmatrix}$$

where

$$s = \frac{1}{2}\left(|\alpha + c_0| + |\alpha - c_0|\right), \quad d = \frac{1}{2}\left(|\alpha + c_0| - |\alpha - c_0|\right)$$

$$s_a = \text{sign}(\alpha), \quad s_\alpha = \frac{1}{2}\left(\text{sign}(\alpha + c_0) + \text{sign}(\alpha - c_0)\right), \quad d_\alpha = \frac{1}{2}\left(\text{sign}(\alpha + c_0) - \text{sign}(\alpha - c_0)\right)$$

For the second kind of stabilization, we have

$$M = \rho_0 I, \quad D = \begin{pmatrix} \rho_0\alpha & 0 & 0 & 0 & n_x \\ 0 & \rho_0\alpha & 0 & 0 & n_y \\ 0 & \rho_0\gamma & \rho_0\alpha_1 & 0 & \beta_x \\ -\rho_0\gamma & 0 & 0 & \rho_0\alpha_1 & \beta_y \\ -(\rho_0 c_0)^2 n_x & -(\rho_0 c_0)^2 n_y & 0 & 0 & \rho_0\alpha \end{pmatrix}$$

The system is diagonizable if $\alpha_1 \neq \alpha, \alpha + c_0, \alpha - c_0$. The eigenvalues and eigenvectors of this system are given as

$$L = \begin{pmatrix} \alpha \\ \alpha_1 \\ \alpha_1 \\ \alpha + c \\ \alpha - c \end{pmatrix}, \quad V = \begin{pmatrix} -n_y(\alpha - \alpha_1) & 0 & 0 & -n_x & n_x \\ n_x(\alpha - \alpha_1) & 0 & 0 & -n_y & n_y \\ \gamma n_x & 1 & 0 & a_{11} & a_{12} \\ \gamma n_y & 0 & 1 & a_{21} & a_{22} \\ 0 & 0 & 0 & \rho_0 c_0 & \rho_0 c_0 \end{pmatrix}$$

where

$$a_{11} = \frac{-\gamma n_y + \beta_x c_0}{\alpha + c_0 - \alpha_1}, \quad a_{12} = \frac{\gamma n_y + \beta_x c_0}{\alpha - c_0 - \alpha_1}, \quad a_{21} = \frac{\gamma n_x + \beta_y c_0}{\alpha + c_0 - \alpha_1}, \quad a_{22} = \frac{-\gamma n_x + \beta_y c_0}{\alpha - c_0 - \alpha_1}$$

The inverse of V is equal to

$$V^{-1} = \begin{pmatrix} \dfrac{-n_y}{\alpha - \alpha_1} & \dfrac{n_x}{\alpha - \alpha_1} & 0 & 0 & 0 \\ \dfrac{n_x}{2}(a_{11} - a_{12}) + \dfrac{\gamma\, n_x\, n_y}{\alpha - \alpha_1} & \dfrac{n_y}{2}(a_{11} - a_{12}) - \dfrac{\gamma\, n_x^2}{\alpha - \alpha_1} & 1 & 0 & -\dfrac{a_{11} + a_{12}}{2\rho_0 c_0} \\ \dfrac{n_x}{2}(a_{21} - a_{22}) + \dfrac{\gamma\, n_y^2}{\alpha - \alpha_1} & \dfrac{n_y}{2}(a_{21} - a_{22}) - \dfrac{\gamma\, n_x\, n_y}{\alpha - \alpha_1} & 0 & 1 & -\dfrac{a_{21} + a_{22}}{2\rho_0 c_0} \\ -\dfrac{n_x}{2} & -\dfrac{n_y}{2} & 0 & 0 & \dfrac{1}{2\rho_0 c_0} \\ \dfrac{n_x}{2} & \dfrac{n_y}{2} & 0 & 0 & \dfrac{1}{2\rho_0 c_0} \end{pmatrix}$$

The absolute matrix of D is given as:

$$|D| = \begin{pmatrix} \rho_0|\alpha| + n_x^2\rho_0(s-|\alpha|) & n_xn_y\rho_0(s-|\alpha|) & 0 & 0 & -\dfrac{dn_x}{c_0} \\ n_xn_y\rho_0(s-|\alpha|) & \rho_0|\alpha| + n_y^2\rho_0(s-|\alpha|) & 0 & 0 & -\dfrac{dn_y}{c_0} \\ \rho_0(-\gamma n_xn_ys_a + n_xb_1) & \rho_0(\gamma n_x^2s_a + n_yb_1) & \rho_0|\alpha_1| & 0 & \dfrac{1}{c_0}(a_{11}d_c + a_{12}d_{-c}) \\ \rho_0(-\gamma n_y^2s_a + n_xb_2) & \rho_0(\gamma n_xn_ys_a + n_yb_2) & 0 & \rho_0|\alpha_1| & \dfrac{1}{c_0}(a_{21}d_c + a_{22}d_{-c}) \\ -\rho_0^2c_0n_xd & -\rho_0^2c_0n_yd & 0 & 0 & \rho_0 s \end{pmatrix}$$

where

$$s = \frac{1}{2}\left(|\alpha + c_0| + |\alpha - c_0|\right), \quad d = \frac{1}{2}\left(|\alpha + c_0| - |\alpha - c_0|\right)$$

$$s_a = \mathrm{sign}(\alpha), \quad d_c = \frac{1}{2}\left(|\alpha + c_0| - |\alpha_1|\right), \quad d_{-c} = \frac{1}{2}\left(|\alpha - c_0| - |\alpha_1|\right)$$

$$b_1 = (-a_{11}d_c + a_{12}d_{-c}), \quad b_2 = (-a_{21}d_c + a_{22}d_{-c})$$

B Linearized Euler Equations

We consider that the background ρ_0, v_0 and p_0 satisfy non-linear Euler equations given as

$$\begin{cases} \partial_t \rho_0 + \operatorname{div}(\rho_0 v_0) = f_\rho \\ \rho_0 \partial_t v_0 + \rho_0 (\nabla v_0) v_0 + \nabla p_0 = f_v \\ \partial_t p_0 + v_0 \cdot \nabla p_0 + \gamma\, p_0 \operatorname{div}(v_0) = f_p \end{cases} \tag{17}$$

We assume that, the fields v_0, ρ_0 and p_0 are steady fields, i.e.

$$\partial_t \rho_0 = \partial_t p_0 = 0, \quad \partial_t v_0 = 0$$

The first equation is linearized as (ρ, p and v are the perturbed fields)

$$\partial_t \rho + \operatorname{div}(\rho v_0) + \operatorname{div}(\rho_0 v) = 0$$

We introduce

$$u = \rho_0 v, \quad M = v_0$$

to obtain

$$(\partial_t + M \cdot \nabla)\rho + \rho \operatorname{div}(M) + \operatorname{div}(u) = 0$$

The second equation is linearized as

$$\rho \partial_t v_0 + \rho (\nabla v_0) v_0 + \rho_0 \partial_t v + \rho_0 (\nabla v_0) v + \rho_0 (\nabla v) v_0 + \nabla p = 0$$

By using $\partial_t v_0 = 0$ and replacing v by u/ρ_0, we obtain

$$\partial_t u + \nabla M(\rho M + u) + \rho_0 \nabla \left(\frac{u}{\rho_0}\right) M + \nabla p = 0$$

and finally

$$(\partial_t + M \cdot \nabla) u + \nabla M(\rho M + u) - \frac{\nabla \rho_0 \cdot M}{\rho_0} u + \nabla p = 0$$

The third equation is linearized as

$$\partial_t p + v_0 \cdot \nabla p + v \cdot \nabla p_0 + \gamma\, p \operatorname{div}(v_0) + \gamma\, p_0 \operatorname{div}(v) = 0$$

which is equal to

$$(\partial_t + M \cdot \nabla) p + \frac{u \cdot \nabla p_0}{\rho_0} + \gamma\, p_0 \operatorname{div}\left(\frac{u}{\rho_0}\right) + \gamma\, p \operatorname{div}(M) = 0$$

We use the relationship

$$\gamma\, p_0 \operatorname{div}\left(\frac{u}{\rho_0}\right) = \operatorname{div}\left(\frac{\gamma\, p_0}{\rho_0} u\right) - p_0 \frac{\nabla \gamma \cdot u}{\rho_0} - \gamma \frac{\nabla p_0 \cdot u}{\rho_0}$$

to obtain the final equation

$$(\partial_t + M \cdot \nabla) p + (1 - \gamma) \frac{u \cdot \nabla p_0}{\rho_0} + \operatorname{div}\left(c_0^2 u\right) + \gamma \operatorname{div}(M)\, p - p_0 \frac{\nabla \gamma \cdot u}{\rho_0} = 0$$

As a result, we obtained Linearized Euler equations given as

$$\begin{cases} (-i\omega + \sigma + M\cdot\nabla)\rho + \rho\,\mathrm{div}\,(M) + \mathrm{div}(u) = 0 \\ (-i\omega + \sigma + M\cdot\nabla)u + \nabla M(\rho M + u) - \dfrac{\nabla\rho_0\cdot M}{\rho_0}u + \nabla p = 0 \\ (-i\omega + \sigma + M\cdot\nabla)p + (1-\gamma)\dfrac{u\cdot\nabla p_0}{\rho_0} + \mathrm{div}\left(c_0^2 u\right) + \gamma\,\mathrm{div}(M)p - p_0\dfrac{\nabla\gamma\cdot u}{\rho_0} = 0 \end{cases} \tag{18}$$

in time-harmonic domain by substituting ∂_t by $-i\omega + \sigma$.

C Axisymmetric computations

C.1 General setting

It is assumed here that the unknowns and background data are expressed in cylindrical coordinates (r, θ, z) :

$$\left\{ \begin{array}{l} x = r\cos\theta \\ y = r\sin\theta \\ z = z \end{array} \right.$$

The orthonormal basis associated with cylindrical coordinates is given as:

$$e_r \;=\; \left[\begin{array}{c} \cos\theta \\ \sin\theta \\ 0 \end{array} \right], \quad e_\theta \;=\; \left[\begin{array}{c} -\sin\theta \\ \cos\theta \\ 0 \end{array} \right], \quad e_z \;=\; \left[\begin{array}{c} 0 \\ 0 \\ 1 \end{array} \right]$$

Moreover, it is assumed that the background data does not depend on θ :

$$\rho_0 = \rho_0(r,z), \quad c_0 = c_0(r,z), \quad p_0 = p_0(r,z), \quad M = m_r(r,z)e_r + m_\theta(r,z)e_\theta + m_z(r,z)$$

An unknown u is decomposed in Fourier series of θ :

$$u \;=\; \sum_{m=-\infty}^{\infty} u^m e^{-im\theta}$$

For a scalar unknown (such as p), the mode u^m is then decomposed in the 2-D finite element space of the section. For a vectorial unknown (such as u or v, the mode u^m is expressed in the basis (e_r, e_θ, e_z):

$$u^m = u_r^m(r,z)e_r + u_\theta^m(r,z)e_\theta + u_z^m(r,z)$$

Under the assumptions made on the background data, the modes $(u_r^m, u_\theta^m, u_z^m)$ are solving independent equations. In the sequel, the superscript m will be omitted and m will be a parameter of the equations.

Galbrun's equation

The formulation PV has been implemented with the two additional unknowns p, v. The equations in cylindrical coordinates are given as:

$$\left\{ \begin{array}{l} \rho_0 \left(-i\omega + \sigma + m_r \dfrac{\partial}{\partial r} - im\dfrac{m_\theta}{r} + m_z \dfrac{\partial}{\partial z} \right) u - \rho_0 v = 0 \\ \rho_0 \left(-i\omega + \sigma + m_r \dfrac{\partial}{\partial r} - im\dfrac{m_\theta}{r} + m_z \dfrac{\partial}{\partial z} \right) v_r - \dfrac{\partial}{\partial r}\left(\rho_0 c_0^2 p\right) + \left(\dfrac{u_r - imu_\theta}{r} + \dfrac{\partial u_z}{\partial z} \right) \dfrac{\partial p_0}{\partial r} - \dfrac{\partial u_z}{\partial r}\dfrac{\partial p_0}{\partial z} = f_r \\ \rho_0 \left(-i\omega + \sigma + m_r \dfrac{\partial}{\partial r} - im\dfrac{m_\theta}{r} + m_z \dfrac{\partial}{\partial z} \right) v_\theta + \dfrac{im}{r}\left(\rho_0 c_0^2 p + u_r \dfrac{\partial p_0}{\partial r} + u_z \dfrac{\partial p_0}{\partial z} \right) = f_\theta \\ \rho_0 \left(-i\omega + \sigma + m_r \dfrac{\partial}{\partial r} - im\dfrac{m_\theta}{r} + m_z \dfrac{\partial}{\partial z} \right) v_z - \dfrac{\partial}{\partial z}\left(\rho_0 c_0^2 p\right) + \left(\dfrac{u_r - imu_\theta}{r} + \dfrac{\partial u_r}{\partial r} \right) \dfrac{\partial p_0}{\partial z} - \dfrac{\partial u_r}{\partial z}\dfrac{\partial p_0}{\partial r} = f_z \\ p - \dfrac{1}{r}\dfrac{\partial (ru_r)}{\partial r} + \dfrac{im}{r}u_\theta - \dfrac{\partial u_z}{\partial z} = 0 \end{array} \right.$$

The formulation PQ has also been implemented and is given as:

$$\begin{cases}
\rho_0\left(-i\omega+\sigma+m_r\dfrac{\partial}{\partial r}-im\dfrac{m_\theta}{r}+m_z\dfrac{\partial}{\partial z}\right)u_r-\dfrac{\partial p}{\partial r}-\rho_0 q_r=0\\
\rho_0\left(-i\omega+\sigma+m_r\dfrac{\partial}{\partial r}-im\dfrac{m_\theta}{r}+m_z\dfrac{\partial}{\partial z}\right)u_\theta+\dfrac{im}{r}p-\rho_0 q_\theta=0\\
\rho_0\left(-i\omega+\sigma+m_r\dfrac{\partial}{\partial r}-im\dfrac{m_\theta}{r}+m_z\dfrac{\partial}{\partial z}\right)u_z-\dfrac{\partial p}{\partial z}-\rho_0 q_z=0\\
\rho_0\left(-i\omega+\sigma+m_r\dfrac{\partial}{\partial r}-im\dfrac{m_\theta}{r}+m_z\dfrac{\partial}{\partial z}\right)q_r-\dfrac{\partial\sigma}{\partial r}p-\left(\dfrac{\partial m_r}{\partial r}\dfrac{\partial p}{\partial r}-\dfrac{im}{r}\dfrac{\partial m_\theta}{\partial r}p+\dfrac{\partial m_z}{\partial r}\dfrac{\partial p}{\partial z}\right)\\
\qquad-\dfrac{M\cdot\nabla\rho_0}{\rho_0}\dfrac{\partial p}{\partial r}+\left(\dfrac{u_r-imu_\theta}{r}+\dfrac{\partial u_z}{\partial z}\right)\dfrac{\partial p_0}{\partial r}-\dfrac{\partial u_z}{\partial r}\dfrac{\partial p_0}{\partial z}=f_r\\
\rho_0\left(-i\omega+\sigma+m_r\dfrac{\partial}{\partial r}-im\dfrac{m_\theta}{r}+m_z\dfrac{\partial}{\partial z}\right)q_\theta+\dfrac{im}{r}\left(\dfrac{M\cdot\nabla\rho_0}{\rho_0}p+u_r\dfrac{\partial p_0}{\partial r}+u_z\dfrac{\partial p_0}{\partial z}\right)=f_\theta\\
\rho_0\left(-i\omega+\sigma+m_r\dfrac{\partial}{\partial r}-im\dfrac{m_\theta}{r}+m_z\dfrac{\partial}{\partial z}\right)q_z-\dfrac{\partial\sigma}{\partial z}p-\left(\dfrac{\partial m_r}{\partial z}\dfrac{\partial p}{\partial r}-\dfrac{im}{r}\dfrac{\partial m_\theta}{\partial z}p+\dfrac{\partial m_z}{\partial z}\dfrac{\partial p}{\partial z}\right)\\
\qquad-\dfrac{M\cdot\nabla\rho_0}{\rho_0}\dfrac{\partial p}{\partial z}+\left(\dfrac{u_r-imu_\theta}{r}+\dfrac{\partial u_r}{\partial r}\right)\dfrac{\partial p_0}{\partial z}-\dfrac{\partial u_r}{\partial z}\dfrac{\partial p_0}{\partial r}=f_z\\
\rho_0\left(-i\omega+\sigma+m_r\dfrac{\partial}{\partial r}-im\dfrac{m_\theta}{r}+m_z\dfrac{\partial}{\partial z}\right)p-(\rho_0c_0)^2\left(\dfrac{u_r-imu_\theta}{r}+\dfrac{\partial u_r}{\partial r}+\dfrac{\partial u_z}{\partial z}\right)=0
\end{cases}$$

Other equations such as LEE or simplified Galbrun's equations are treated in a similar fashion.

C.2 Numerical results

A non-uniform flow is chosen:

$$\rho_0=1.6+0.3\cos\left(\frac{\pi r}{4}\right)\sin\left(\frac{\pi z}{4}\right)$$

$$c_0=1.2+0.2\left(\frac{r^2}{10}+\sin\left(\frac{\pi r}{4}\right)\cos\left(\frac{\pi z}{4}\right)\right)$$

$$p0=2.2+0.4\sin\left(\frac{\pi r}{4}\right)\cos\left(\frac{\pi z}{4}\right)$$

$$m_r=m_\theta=0,\quad m_z=\frac{\mathrm{C}}{\rho_0}\cos\left(\frac{\pi r}{4}\right)$$

The constant C will depend on the numerical experiment considered. The computational domain is the rectangle $[0,4]\times[-4,4]$ corresponding to a cylinder in 3-D. A zero-order absorbing boundary condition is set on the lateral boundary $r=4$ whereas periodic conditions are imposed for $z=\pm4$. The source g is a gaussian centered at the origin with a radius of distribution equal to 1, and polarized in the x-direction. This source is decomposed exactly in the two modes $m=\pm1$. The solutions obtained for Galbrun's equations and LEE are displayed in figures 36, 37, 38 and 39 for different values of the constant C. These solutions can be compared since the relation

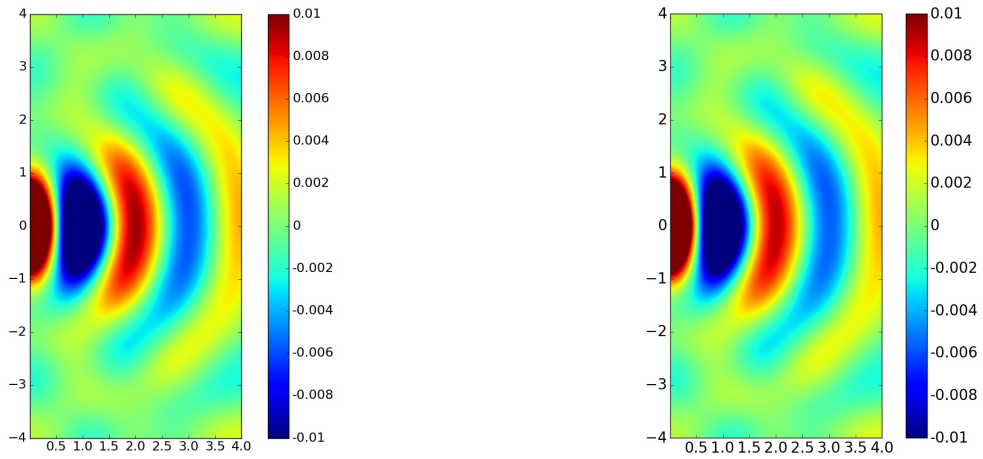

Figure 36: Solution obtained with Galbrun's equation (left) and LEE (right) ($C = 0$, real part of u_x in plane Oxz).

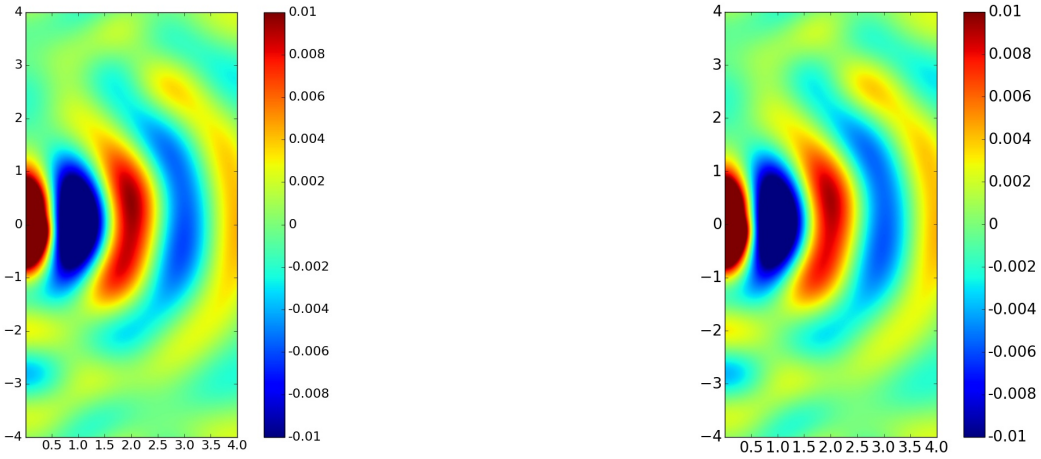

Figure 37: Solution obtained with Galbrun's equation (left) and LEE (right) ($C = 0.1$, real part of u_x in plane Oxz).

$$f \;=\; (-i\omega + \sigma + M \cdot \nabla)g$$

is satisfied. The consistency errors are displayed in figures 40 and 42, while the L^2 errors between the solution and a reference solution are plotted in figures 41 and 43. The results are similar to the 2-D case, Galbrun's equations progressively do not converge for larger values of the flow, whereas linearized Euler Equations exhibit a nice convergence. When we are using simplified

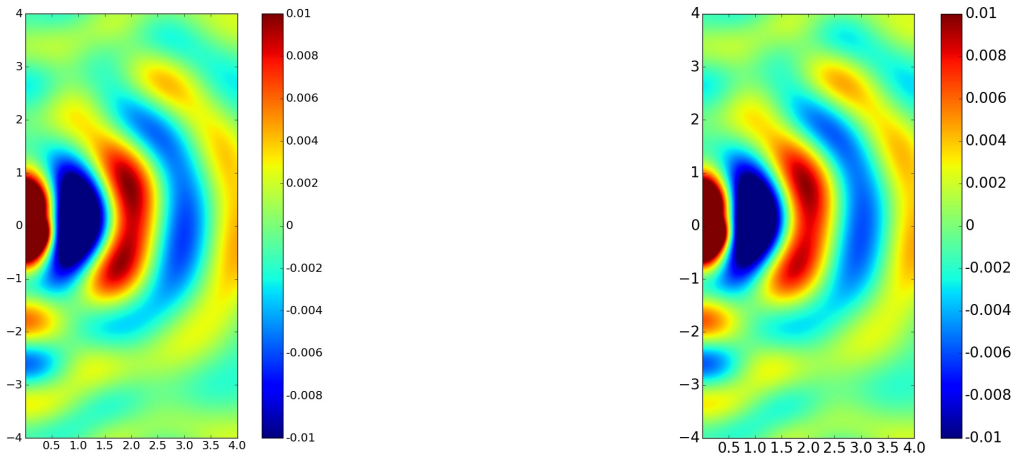

Figure 38: Solution obtained with Galbrun's equation (left) and LEE (right) ($C = 0.2$, real part of u_x in plane Oxz).

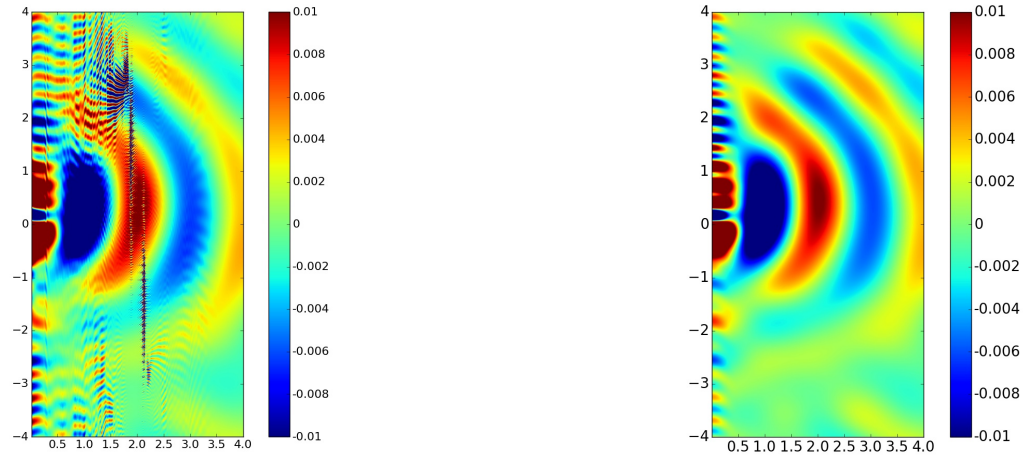

Figure 39: Solution obtained with Galbrun's equation (left) and LEE (right) ($C = 0.5$, real part of u_x in plane Oxz).

Galbrun's equation, we have also observed a good convergence.

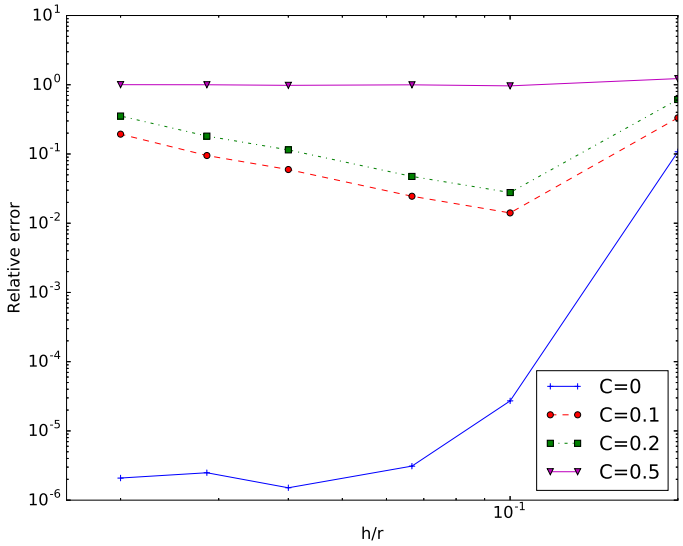

Figure 40: Consistency error for Galbrun's equation and different values of C.

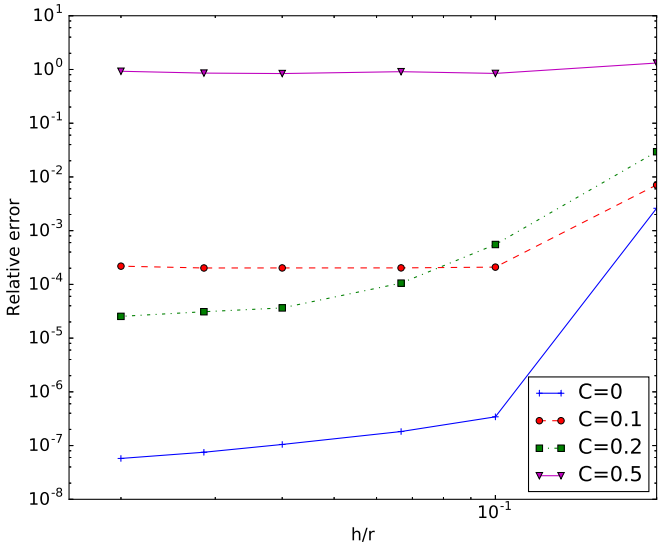

Figure 41: Relative L^2 error for Galbrun's equation and different values of C.

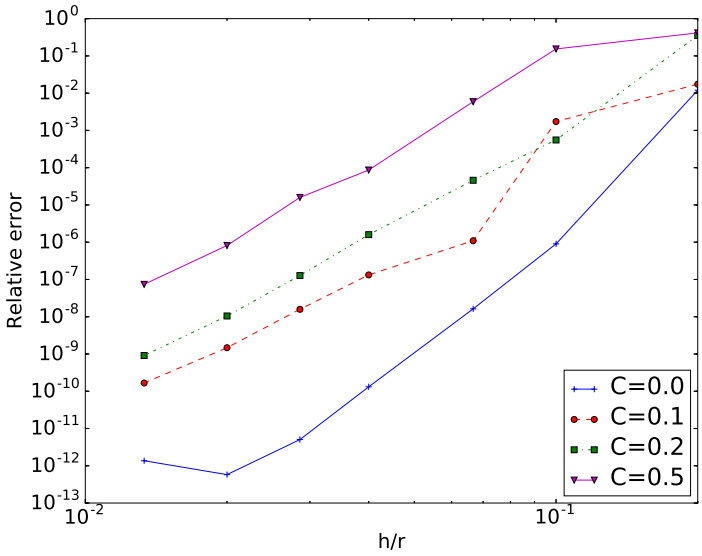

Figure 42: Consistency error for LEE and different values of C.

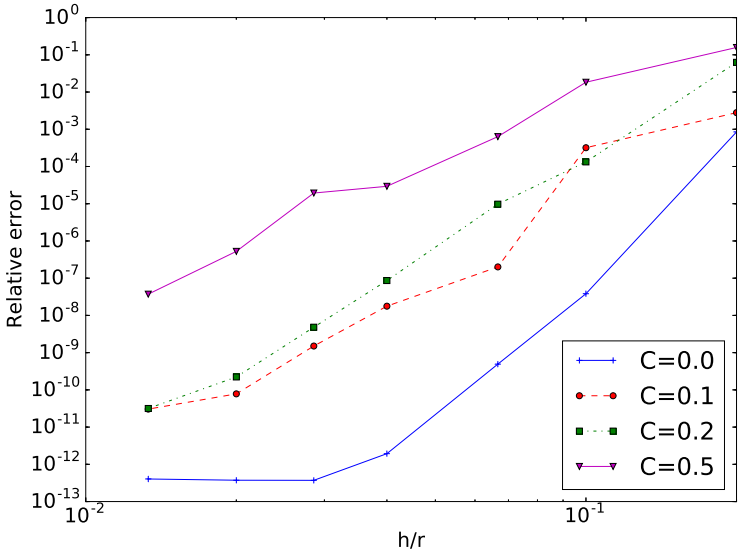

Figure 43: Relative L^2 error for LEE and different values of C.

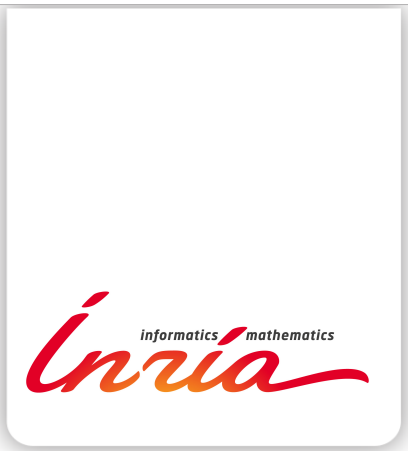

RESEARCH CENTRE
BORDEAUX – SUD-OUEST

200 avenue de la Vieille Tour
33405 Talence Cedex

Publisher
Inria
Domaine de Voluceau - Rocquencourt
BP 105 - 78153 Le Chesnay Cedex
inria.fr

ISSN 0249-6399